Chemical Geology 561 (2021) 120031

Contents lists available at ScienceDirect

Chemical Geology

journal homepage: www.elsevier.com/locate/chemgeo

Theoretical calculation of position-specific carbon and hydrogen isotope equilibriums in butane isomers

Qi Liu [a], Xinya Yin [b], Yining Zhang [a], Maxime Julien [c], Naizhong Zhang [d], Alexis Gilbert [c,d], Naohiro Yoshida [d,e], Yun Liu [a,f,*]

[a] State Key Laboratory of Ore Deposit Geochemistry, Institute of Geochemistry, Chinese Academy of Sciences, Guiyang 550081, China
[b] Guizhou Minzu University, Guiyang 550025, China
[c] Department of Earth and Planetary Sciences, Tokyo Institute of Technology, Tokyo 152-8551, Japan
[d] Earth-Life Science Institute, Tokyo Institute of Technology, Tokyo 152-8550, Japan
[e] National Institute of Information and Communications Technology, Tokyo 184-8795, Japan
[f] International Center for Planetary Science, College of Earth Sciences, Chengdu University of Technology, Chengdu 610059, China

ARTICLE INFO

Editor: Michael E. Boettcher

Keywords:
Position-specific isotope effects
Intramolecular isotope
Carbon isotopes
Hydrogen Isotopes
Equilibrium isotope effects
Butane isomers

ABSTRACT

Position-specific isotope analysis has shown its potential to reveal information regarding formation, migration, and conversion procesess of hydrocarbons. The intramolecular isotope compositions of butane are promising to serve as a new thermometer and tracer. Therefore, position-specific isotope signatures in butane at equilibrium are needed for calibrating experimental measurements, establishing new geothermometers, and recognizing kinetic isotope effects. Here we conduct quantum chemistry modeling with corrections beyond the harmonic approximation and the Born-Oppenheimer approximation to obtain accurate intramolecular and intermolecular carbon and hydrogen isotope fractionation factors for butane isomers at equilibrium. Temperature dependences of these equilibrium isotope effects are presented for the range from 0 °C to 726.85 °C. The contribution of higher-order energy terms to 1000lnα values beyond the Bigeleisen-Mayer equation is found to be comparable to the magnitude of current experimental precisions. In addition to the significance of anharmonicity, the contribution of hindered internal rotation and diagonal Born-Oppenheimer correction is found to be important for accurate predictions of position-specific hydrogen isotope equilibriums. The abundance ratio of *n*-butane to *i*-butane at equilibriums is also calculated at various temperatures. Our results provide fundamental understanding of equilibrium properties for studying position-specific isotope effects in butane.

1. Introduction

Position-specific isotope effects (PSIEs, sometimes called site-specific isotope effects) describe intramolecular isotope fractionations arising from isotope substitutions at the non-equivalent positions in a molecule (Eiler, 2013). For example, carbon sites of the methyl and carboxyl groups within acetic acid, which are non-equivalent positions, have their unique isotope signatures ($\delta^{13}C_{methyl}$ and $\delta^{13}C_{carboxyl}$, respectively) and the difference between their $\delta^{13}C$ values ($\Delta^{13}C_{carboxyl\text{-}methyl} = \delta^{13}C_{carboxyl} - \delta^{13}C_{methyl}$) expresses the intramolecular ^{13}C distribution within acetic acid. Since methyl and carboxyl groups participate differently in (bio)chemical reactions or physical processes, the "bulk" isotope effects measured using conventional methods (compound-specific isotope analysis, CSIA) reflect an average isotopic composition of these two carbon positions (Yamada et al., 2014).

The study of position-specific isotope effects can be tracked back to several decades ago. Abelson and Hoering (1961) measured the intramolecular carbon isotope fractionation in amino acids, and found the carboxyl carbon positions are isotopically enriched relative to the rest. This work triggered the further analyses and implements of position-specific isotope effects (e.g., Corso and Brenna, 1997; Melzer and Schmidt, 1987; Monson and Hayes, 1980, 1982a,b; Vogler and Hayes, 1980). With the technological advances of mass spectrometry (MS) and nuclear magnetic resonance (NMR) spectroscopy, position-specific isotope analysis (PSIA) has shown its great potential to trace the origin or the formation mechanism of substances. For example, position-specific nitrogen isotope effects served as a valuable tracer to constrain global budget of N_2O (Yoshida and Toyoda, 2000). Position-specific

* Corresponding author at: State Key Laboratory of Ore Deposit Geochemistry, Institute of Geochemistry, Chinese Academy of Sciences, Guiyang 550081, China.
E-mail address: liuyun@vip.gyig.ac.cn (Y. Liu).

https://doi.org/10.1016/j.chemgeo.2020.120031
Received 27 September 2020; Received in revised form 15 December 2020; Accepted 15 December 2020
Available online 17 December 2020

hydrogen isotope analysis has been utilized for determinations of illicit drugs (Armellin et al., 2006; Brenna et al., 2007). The position-specific carbon isotope analysis, such as $\delta^{13}C$ values of methyl carbons and other carbon sites, can provide unique information to differentiate the sources of functional groups (Bayle et al., 2014; Gilbert et al., 2013a,b; Hattori et al., 2011). The development of the position-specific carbon isotope analysis for propane makes it possible to improve our understanding of the formation of natural gases and their isotopic variations (Gao et al., 2016; Gilbert et al., 2016a; Li et al., 2018; Liu et al., 2018; Piasecki et al., 2016a, 2018). Recently, Xie et al. (2018) catalyzed position-specific hydrogen isotope equilibrium in propane, and demonstrated the possibility of using position-specific hydrogen isotope analysis as a new geothermometer. Gilbert et al. (2019) found anaerobic microbial degradation of propane produced position-specific carbon isotope anomalies in propane, and extended the application of PSIA to identify anaerobic microbial oxidation processes in natural settings. Liu et al. (2019) showed both position-specific carbon and hydrogen isotope effects in propane from natural gases with high accuracy and illustrated the potential applications of position-specific isotope effects in other hydrocarbon gases.

Considering that the techniques can be expanded to analyze larger hydrocarbons (e.g., Gilbert et al., 2016b; Liu et al., 2018), the position-specific isotope effects in butane would draw much attention in the upcoming studies. Butane (C_4H_{10}), the gaseous alkane at room temperature and atmospheric pressure, is one component of natural gas (Claypool and Kvenvolden, 1983), an atmospheric organic pollution on Earth (Schauer et al., 1999), and an important compound in chemical and petrochemical industries (e.g., Zhang et al., 2008). Butane also represents a typical hydrocarbon with an abiotic origin under deep Earth conditions (Huang et al., 2017; Kolesnikov et al., 2009, 2017), and an astrophysical molecule on extraterrestrial planets and their satellites (Curtis et al., 2005; Dobrijevic et al., 2016; Murphy et al., 2003). Butane has two structural isomers: normal butane (*n*-butane) and isobutane (*i*-butane, also called 2-methylpropane). Because of the structural difference, *n*-butane and *i*-butane differ in physical and chemical properties, such as their stabilities and isotopic enrichments. Meanwhile, normal butane has two conformers due to the rotational isomerization: the *trans* (*anti*) form and the *gauche* form. The *trans* and *gauche* forms of *n*-butane co-exist in a conformational equilibrium, where their abundances are temperature dependent. These properties make butane system a potentially useful proxy for geochemical studies. Very recently, Julien et al. (2020) demonstrated position-specific ^{13}C variations in *n*-butane and *i*-butane with their newly developed analytical method, lightening the further application of intramolecular isotope effects in butane isomers.

In the near future, we would expect that there are increasing studies of position-specific isotope effects to contribute fundamental knowledge for geoscience, forensic science, pharmacological science, food science, etc. (Eiler, 2013). Therefore, the combination of theoretical work and experimental analysis has to be strengthened to make these studies step further. Especially, it is imperative to obtain accurate equilibrium position-specific isotope fractionation factors for calibrating geothermometry and identifying kinetic processes.

Although several theoretical studies have shown equilibrium position-specific isotope fractionation factors (Galimov, 1985; Galimov and Ivlev, 1973; He et al., 2020; Piasecki et al., 2016b; Polyakov and Horita, 2021; Rustad, 2009; Wang et al., 2009a, 2013; Webb and Miller III, 2014), none of their results can be directly used for comparing the temperature dependences of intramolecular carbon and hydrogen isotope equilibriums in butane isomers. For example, Galimov (1985, 2006) used "isotopic bond numbers" method to provide position-specific isotope fractionation factors only for carbon isotope equilibriums. Wang et al. (2009a) and He et al. (2020) predicted equilibrium position-specific hydrogen or carbon isotope fractionations for large organic molecules based on the "cutoff" effects respectively. However, for building a hydrogen isotope or carbon isotope thermometer, these results are not accurate enough for smaller hydrocarbons such as propane or butane. In this study, we calculate position-specific carbon and hydrogen isotope equilibriums for both *n*-butane and *i*-butane by using methods beyond the harmonic approximation and the Born-Oppenheimer approximation. The contributions of energy terms from anharmonicities, non-rigid rotations, and adiabatic corrections are carefully investigated. Accurate temperature dependences of intramolecular and intermolecular isotope equilibriums within and between butane isomers are provided.

2. Methods

2.1. Theoretical calculation of equilibrium isotope fractionation

For an isotope equilibrium of single substitution,

$$AX^1X^2 + X^* = AX^{*1}X^2 + X \tag{1}$$

where AX^1X^2 (formula AX_2), containing no heavy isotopes, has two non-equivalent positions of element X (position 1 and position 2, respectively), X^* means the heavy isotope of element X, $AX^{*1}X^2$ represents the isotopologue that X^* substituted at the position 1. The reduced partition function ratio for calculating isotope equilibrium of this reaction can be expressed by the Bigeleisen-Mayer equation using the β factor (Bigeleisen and Mayer, 1947; Galimov, 2006; Liu et al., 2010; Schauble, 2004; Urey, 1947):

$$\begin{aligned}\beta_1(AX_2) = \beta\left(AX^{*1}X^2/AX^1X^2\right) &= \frac{s_{AX^{*1}X^2}}{s_{AX^1X^2}}\frac{Q_{AX^{*1}X^2}}{Q_{AX^1X^2}}\Big/\frac{Q_{X^*}}{Q_X} \\ &= \prod_i \frac{u_i\left(AX^{*1}X^2\right)exp\left[-u_i\left(AX^{*1}X^2\right)/2\right]\left\{1-exp\left[-u_i\left(AX^1X^2\right)\right]\right\}}{u_i\left(AX^1X^2\right)exp\left[-u_i\left(AX^1X^2\right)/2\right]\left\{1-exp\left[-u_i\left(AX^{*1}X^2\right)\right]\right\}}\end{aligned} \tag{2}$$

Q represents partition function, i.e., Q_X means the partition function of X. s means symmetry number. $u_i = hc\omega_i/k_BT$ where h is the Planck constant, c is the speed of light in vacuum, ω_i is the harmonic frequency of normal mode i in the unit of cm^{-1}, k_B is the Boltzmann constant and T is absolute temperature. The position-specific isotope fractionation factor α at equilibrium arising from isotope substitutions at individual positions can be expressed as the ratio of their β factors:

$$\alpha_{2-1} = \frac{\beta_2}{\beta_1} \tag{3}$$

When one calculates isotope equilibriums between two compounds, an arithmetic average of β factors can be utilized if a molecule has n positions (not non-equivalent positions) for isotope substitutions (Galimov, 2006):

$$\beta_{AX_n} = \frac{1}{n}\sum_i^n \beta_i(AX_n) \tag{4}$$

then,

$$\alpha_{AX_n-BX_m} = \frac{m}{n}\frac{\beta_{AX_n}}{\beta_{BX_m}} \tag{5}$$

Therefore, we consider the following reactions for calculating carbon and hydrogen isotope equilibriums in butane isomers,

$$^{12}CH_3{}^{12}CH_2{}^{12}CH_2{}^{12}CH_3 + {}^{13}C = {}^{13}CH_3{}^{12}CH_2{}^{12}CH_2{}^{12}CH_3 + {}^{12}C \tag{A1}$$

$$^{12}CH_3{}^{12}CH_2{}^{12}CH_2{}^{12}CH_3 + {}^{13}C = {}^{12}CH_3{}^{13}CH_2{}^{12}CH_2{}^{12}CH_3 + {}^{12}C \tag{A2}$$

$$^{12}CH_3{}^{12}CH_2{}^{12}CH_2{}^{12}CH_3 + D = {}^{12}CH_2D{}^{12}CH_2{}^{12}CH_2{}^{12}CH_3 + H \tag{B1}$$

$$^{12}CH_3{}^{12}CH_2{}^{12}CH_2{}^{12}CH_3 + D = {}^{12}CH_3{}^{12}CHD{}^{12}CH_2{}^{12}CH_3 + H \tag{B2}$$

$$^{12}CH_3{}^{12}CH\left({}^{12}CH_3\right){}^{12}CH_3 + {}^{13}C = {}^{13}CH_3{}^{12}CH\left({}^{12}CH_3\right){}^{12}CH_3 + {}^{12}C \tag{C1}$$

$$^{12}CH_3{}^{12}CH(^{12}CH_3)^{12}CH_3 + {}^{13}C = {}^{12}CH_3{}^{13}CH(^{12}CH_3)^{12}CH_3 + {}^{12}C \quad (C2)$$

$$^{12}CH_3{}^{12}CH(^{12}CH_3)^{12}CH_3 + D = {}^{12}CH_2D{}^{12}CH(^{12}CH_3)^{12}CH_3 + H \quad (D1)$$

$$^{12}CH_3{}^{12}CH(^{12}CH_3)^{12}CH_3 + D = {}^{12}CH_3{}^{12}CD(^{12}CH_3)^{12}CH_3 + H \quad (D2)$$

Here, A, B, C, and D denote four kinds of isotope exchange reactions, 1 and 2 refer in particular to the non-equivalent positions for isotope substitutions. For example, position 1 and 2 in *n*-butane belong to methyl (CH_3-) group and methylene (-CH_2-) group, respectively.

2.2. Isotope effects from higher-order energy corrections

The Bigeleisen-Mayer equation is derived based on the harmonic approximation and the Born-Oppenheimer approximation. However, corrections beyond these approximations are recommended to obtain more accurate predictions of isotope effects, especially for those reactions containing hydrogen isotope exchanges (Bron et al., 1973; Liu et al., 2010; Richet et al., 1977; Webb and Miller III, 2014). In this study, we considered eight higher-order corrections to the Bigeleisen-Mayer equation when estimating the intramolecular isotope equilibriums in butane. These include the anharmonic correction for zero-point energy, anharmonic correction for vibrational excited states, vibration-rotation coupling correction for zero-point energy, vibration-rotation coupling correction for vibrational excited states, quantum mechanical correction to rotation, centrifugal distortion correction, hindered internal rotation correction, and diagonal Born-Oppenheimer correction. We define the results of those corrections contributing to β factors as AnZPE, AnEXC, VrZPE, VrEXC, QmCorr and CenDist, HIR, and DBOC, respectively (Liu et al., 2010; Zhang and Liu, 2018, and the equations and citations within). The β factor corrected by considering these corrections is distinguished by a superscript "*Corr*", i.e.,

$$\beta^{Corr} = \beta \cdot \text{AnZPE} \cdot \text{AnEXC} \cdot \text{VrZPE} \cdot \text{VrEXC} \cdot \text{QmCorr} \cdot \text{CenDist} \cdot \text{HIR} \cdot \text{DBOC} \quad (6)$$

2.3. Computational details

We use the CCSD(T) method (Pople et al., 1987; Purvis and Bartlett, 1982) with the 6–311+G(d,p) basis set (Frisch et al., 1984; Krishnan et al., 1980; McLean and Chandler, 1980) for geometry optimizations, single-point energy calculations, harmonic frequency generations and hindered internal rotation analyses, and extra MP2/6–311+G(d,p) (Møller and Plesset, 1934) for the calculations of higher-order energy terms. Gaussian 09 package (Frisch et al., 2013) is used to perform all calculations except for DBOC. For the computation of DBOC, the CFOUR package (CFOUR, 2000; Harding et al., 2008a,b) is used based on the optimized butane structures. The calculation of hindered internal rotation is adopted by the treatment of McClurg et al. (1997) and McClurg (1999). "Very tight" geometry convergence criteria and "superfine" grids built in Gaussian 09 are applied for geometry optimization procedures and further computations. Because butane contains equivalent carbon and hydrogen positions, we consider all cases in which that isotope is substituted at different equivalent positions and use the average results (Liu and Liu, 2016). For example, the results of $^{12}CDH_2$-, $^{12}CHDH$- and $^{12}CH_2D$- are averaged when we handle deuterium substituted methyl groups. Furthermore, harmonic frequencies at MP2/6–311+G(d,p) (Møller and Plesset, 1934) and B3LYP/6–311+G(d,p) (Becke, 1993; Lee et al., 1988) are obtained to constrain the uncertainty of β factors calculated on the harmonic approximation.

3. Results

3.1. Frequencies and scale factor

Frequencies calculated at CCSD(T)/6–311+G(d,p), MP2/6–311+G(d,p), B3LYP/6–311+G(d,p) are compared with the experimental fundamentals (see "Exp.^{F}", Bernath et al., 2019; Shimanouchi, 1977) of *trans*, *gauche* and *iso* butane (Table 1). MP2^F means the calculated fundamental frequencies at MP2/6–311+G(d,p), other calculated frequencies (without the superscript *F*) are harmonic frequencies. Among the calculated harmonic frequencies, the results obtained at MP2/6–311+G(d,p) level are larger than these of CCSD(T)/6–311+G(d,p), while B3LYP/6–311+G(d,p) predicts smaller harmonic frequencies than CCSD(T)/6–311+G(d,p) does. Meanwhile, the fundamentals calculated at MP2/6–311+G(d,p) level are systemically larger than the experimental ones. These findings suggest that we may use a frequency scale factor to ensure the accuracy of our calculation at MP2/6–311+G(d,p) level. We therefore presented a correlation relationship between calculated and experimental fundamentals in Fig. 1. A linear least squares regression gives a slope of 1.0186 with a standard error of 0.0013 and an R-squared value of 0.9998. According to the regression line, a frequency scale factor of 0.9816 is estimated for MP2/6–311+G(d,p) level. This scale factor, which is slightly larger than the scale factor 0.9768 estimated by Merrick et al. (2007) for zero-point vibrational energy, will be employed to scale the harmonic frequencies at MP2/6–311+G(d,p) level to obtain the β factors with frequency scaling (distinguished by a superscript of "*sf*"). Because this scale factor is estimated for the normal modes, we do not scale any of our higher-order energy terms when we calculated the corrections (Liu and Liu, 2016). More discussion on the scale factor and related uncertainties can be found in Section 4.1.

3.2. β factor and corrections

Table 2 shows the β factors calculated at CCSD(T), MP2, and B3LYP methods with 6–311+G(d,p) basis set on the harmonic approximation. MP2^{sf} means the β factors calculated on the harmonic approximation with frequency scaling by a factor of 0.9816. The β factors, which are temperature dependent, decrease as temperature increases. Among the β factors without frequency scaling, CCSD(T)/6–311+G(d,p) predicts β factors very close to the mean value of the three sets of data, MP2/6–311+G(d,p) predicts the largest β factors, B3LYP/6–311+G(d,p) predicts the smallest ones. Although there are deviations between the β factors obtained from the computational levels, CCSD(T), MP2, and B3LYP show consistent results with standard deviations of ~ 0.003 and ~ 0.26 for carbon and hydrogen isotope substitutions at 50 °C, and the deviations decrease with temperature increases. Meanwhile, The frequency-scaled MP2/6–311+G(d,p) model (MP2^{sf}), provides the smallest predictions for hydrogen isotope equilibriums among these harmonic β factors. We note that the β factors of B3LYP and MP2^{sf} are very close to each other. The β factors of CCSD(T) and MP2^{sf} have deviations within 0.003 and 0.3 for carbon and hydrogen isotope substitutions during the considered temperature range.

Higher-order corrections to β factors calculated at MP2/6–311+G(d,p) level are listed in Table 3. Except VrZPE, all other corrections to β factors are temperature dependent. AnZPE and DBOC contribute significantly to both carbon and hydrogen isotope substitutions. However, we note AnZPE contributes similarly to the non-equivalent carbon/hydrogen positions in butane isomers, therefore much of the contributions will be canceled when we calculate intramolecular isotope effects. AnEXC contributes less but discrepantly to the non-equivalent positions, especially for hydrogen isotope exchanges, therefore plays an important role in this study. Because the molecular mass of butane is large enough, the higher-order corrections related to rotation become insignificant, i.e., VrZPE and VrEXC show much less contributions and the contributions of QmCorr and CenDist are negligible. The contributions of HIR are significant only for hydrogen isotope substitutions at the terminal

Table 1
Comparison of theoretical and experimental frequencies (cm^{-1}) of *trans-, gauche-, and i-butane.*

trans-butane						*gauche*-butane						*i*-butane					
mode	**CCSD(T)**	**B3LYP**	**MP2**	**MP2^F**	**Exp.^{F}**	**mode**	**CCSD(T)**	**B3LYP**	**MP2**	**MP2^F**	**Exp.^{F}**	**mode**	**CCSD(T)**	**B3LYP**	**MP2**	**MP2^F**	**Exp.^{F}**
CH_3 d-str	3103	3081	3157	3022	2965	CH_3 d-str	3113	3090	3168	3032	2968	CH_3 a-str	3095	3077	3147	3012	2969
CH_3 s-str	3024	3016	3067	2977	2872	CH_3 d-str	3098	3078	3152	3018	2968	CH s-str	3020	3017	3064	2945	2917
CH_2 s-str	3014	2998	3057	2983	2853	CH_2 a-str	3056	3035	3109	2975	2920	CH_3 s-str	3014	3009	3058	2898	2892
CH_3 d-deform	1513	1505	1523	1478	1460	CH_3 s-str	3028	3020	3070	2987	2870	CH_3 a-bend	1522	1514	1532	1488	1478
CH_2 scis	1495	1488	1503	1453	1442	CH_2 s-str	3018	3003	3062	2972	2860	CH_3 s-bend	1437	1428	1439	1404	1397
CH_3 s-deform	1423	1411	1425	1389	1382	CH_3 d-deform	1521	1511	1531	1484	1460	CH_3 rock	1222	1208	1227	1196	1189
CH_2 wag	1411	1393	1412	1371	1361	CH_3 d-deform	1511	1505	1520	1476	1460	CC str	811	795	823	806	797
CH_3 rock	1179	1167	1188	1159	1151	CH_2 scis	1495	1488	1503	1459	1450	CCC bend	431	432	435	438	432
CC str	1087	1063	1102	1076	1059	CH_3 s-deform	1424	1413	1426	1391	1380	CH_3 a-str	3095	3078	3149	3014	none
CC str	851	839	862	848	837	CH_2 wag	1392	1376	1394	1354	1350	CH_3 a-bend	1489	1482	1497	1456	none
CCC deform	424	424	429	427	425	CH_2 twist	1318	1314	1327	1294	1281	CH_3 rock	959	956	965	950	945
CH_3 d-str	3100	3079	3155	3018	2968	CH_3 rock	1205	1193	1211	1183	1168	CH_3-CH torsion	194	212	200	211	225
CH_2 a-str	3063	3039	3118	2981	2930	CC str	1105	1084	1120	1094	1077	CH_3 a-str	3099	3081	3152	3017	2967
CH_3 d-deform	1508	1500	1518	1475	1461	CH_3 rock	998	992	1006	989	980	CH_3 a-str	3099	3081	3152	3017	2967
CH_2 twist	1296	1289	1304	1268	1257	CC str	842	832	853	837	827	CH_3 a-str	3085	3068	3140	3005	2945
CH_3 rock	962	964	969	955	948	CH_2 rock	803	792	812	799	788	CH_3 a-str	3085	3068	3140	3005	2945
CH_2 rock	737	737	746	740	731	CCC deform	318	322	323	323	320	CH_3 s-str	3014	2992	3055	2982	2952
CH_3-CH_2 torsion	223	221	230	222	194	CH_3-CH_2 torsion	275	252	281	262	201	CH_3 s-str	3014	3009	3055	2983	2952
CH_2-CH_2 torsion	109	118	114	118	102	CH_2-CH_2 torsion	110	115	115	108	101	CH_3 a-bend	1513	1507	1523	1480	1477
CH_3 d-str	3096	3075	3152	3017	2965	CH_3 d-str	3104	3083	3160	3025	2968	CH_3 a-bend	1513	1507	1523	1480	1477
CH_2 a-str	3042	3017	3097	2960	2912	CH_3 d-str	3099	3079	3153	3018	2968	CH_3 a-bend	1495	1489	1504	1464	1471
CH_3 d-deform	1508	1499	1518	1473	1460	CH_2 a-str	3061	3037	3115	2978	2920	CH_3 a-bend	1495	1489	1504	1464	1471
CH_2 twist	1333	1332	1343	1311	1300	CH_3 s-str	3026	3018	3067	2992	2870	CH_3 s-bend	1414	1400	1414	1378	1372
CH_3 rock	1220	1207	1225	1195	1180	CH_2 s-str	3016	3002	3061	2975	2860	CH_3 s-bend	1414	1400	1414	1378	1372
CH_2 rock	814	813	821	816	803	CH_3 d-deform	1513	1507	1522	1479	1460	CCH bend	1367	1358	1370	1335	1331
CH_3-CH_2 torsion	255	259	262	254	225	CH_3 d-deform	1507	1499	1517	1471	1460	CCH bend	1367	1358	1370	1335	1331
CH_3 d-str	3103	3082	3157	3022	2968	CH_2 scis	1491	1486	1498	1458	1450	CC str	1203	1190	1213	1183	1174
CH_3 s-str	3026	3017	3067	2988	2870	CH_3 s-deform	1428	1414	1430	1393	1380	CC str	1203	1190	1213	1183	1174
CH_2 s-str	3020	3006	3064	2980	2853	CH_2 wag	1377	1375	1381	1347	1370	CC str	990	971	1001	978	964
CH_3 d-deform	1518	1512	1526	1484	1461	CH_2 twist	1295	1289	1303	1272	1233	CC str	990	971	1001	978	964
CH_2 scis	1499	1492	1508	1463	1461	CC str	1163	1152	1169	1142	1133	CH_3 rock	928	925	935	924	919
CH_3 s-deform	1424	1413	1426	1391	1379	CH_3 rock	980	972	994	971	980	CH_3 rock	928	925	935	924	919
CH_2 wag	1324	1324	1327	1295	1290	CH_3 rock	969	962	976	964	955	CCC bend	363	365	367	369	366
CC str	1035	1015	1049	1023	1009	CH_2 rock	748	752	755	752	747	CCC bend	364	365	367	369	366
CH_3 rock	981	980	988	972	964	CCC deform	436	434	440	434	469	CH_3-CH torsion	260	257	268	263	280
CCC deform	254	258	258	260	271	CH_3-CH_2 torsion	213	215	217	212	197	CH_3-CH torsion	261	257	268	263	280

Our calculated frequencies have been rounded to the nearest integer. Superscript *F* represents fundamental frequencies, i.e., MP2^F means the fundamental frequencies calculated from MP2/6–311+G(d,p) by using $\nu_i = \omega_i + 2x_{ii} + 0.5\sum x_{ij}$ (ν_i is the fundamental frequency at mode *i*, x_{ii} and x_{ij} are anharmonic constants). Exp.^{F} means the experimental fundamentals (Bernath et al., 2019; Shimanouchi, 1977). Others without superscript means the harmonic frequencies calculated at the individual methods. s: symmetrical, a: antisymmetrical, d: degenerate, str: stretching, deform: deformation, rock: rocking, twist: twisting, wag: wagging, scis: scissors, bend: bending.

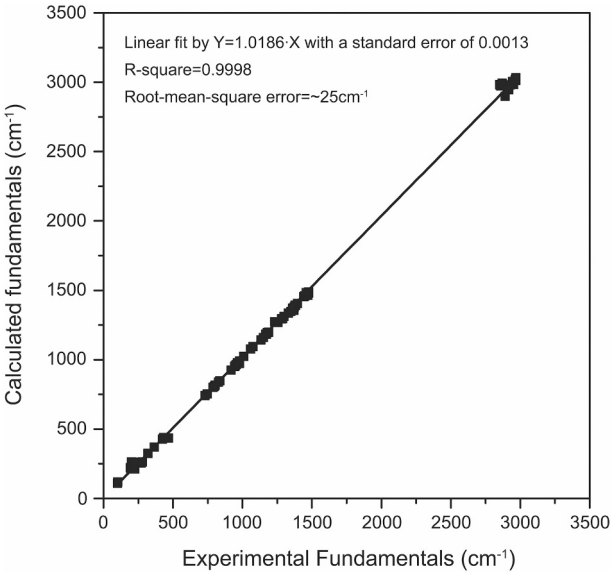

Fig. 1. Comparison of calculated fundamentals (MP2) with experimental ones. The linear least squares regression gives a slope of 1.0186 with an intercept of 0.

positions (in the methyl groups of butane), therefore are of importance for the calculation of intramolecular hydrogen isotope effects. DBOC contributes similarly to the non-equivalent carbon positions in butane isomers, and much of the contributions should be canceled at the calculation of carbon isotope effects.

3.3. Intramolecular and intermolecular equilibrium isotope fractionation

Table 4 shows the intramolecular carbon and hydrogen isotope equilibriums of *trans*-butane, *gauche*-butane and *i*-butane calculated at CCSD(T), MP2 and B3LYP with 6–311+G(d,p) basis set. On the harmonic approximation, CCSD(T) method generates intramolecular isotope fractionations at equilibriums similar to MP2 although the β factors determined from CCSD(T) are smaller than those MP2 predicts. The frequency-scaled MP2 model ($MP2^{sf}$) shows slightly smaller predictions of isotope fractionation factors than the MP2 method. B3LYP method predicts smaller $1000\ln\alpha_{2-1}$ than those of CCSD(T) and MP2 methods for intramolecular carbon isotope equilibriums, but relatively larger for intramolecular hydrogen isotope equilibriums. Meanwhile, the corrections show negative contribution to $1000\ln\alpha_{2-1}(^{13}C/^{12}C)$ values and positive contribution to $1000\ln\alpha_{2-1}$(D/H) values at equilibriums. Because CCSD(T) method stands as a "gold standard" of quantum chemistry but the frequency-scaled MP2 method ($MP2^{sf}$) may be affected by the accuracy of experimental fundamentals (Liu and Liu, 2016), we have reasons to believe that CCSD(T) method can produce very accurate α values (Riley et al., 2010) and choose the results of CCSD(T) as our standard on the harmonic approximation. Therefore, when we combined the harmonic results of CCSD(T) with the effects of corrections, the corrected results ($CCSD(T)^{Corr}$) provide closer predictions to the results of B3LYP method, and show a fractionation crossover of intramolecular carbon isotope equilibriums near 500 °C for *n*-butane. We found the position-specific isotope fractionation factors in *trans*-butane and *gauche*-butane are quite similar when they reach isotope equilibriums, therefore the isotope signature of *trans*-butane can be used to represent that of *n*-butane because of its more abundance at equilibrium. Furthermore, our results show that the equilibrium position-specific isotope fractionation factor of *i*-butane is almost twice the value of *n*-butane for either carbon or hydrogen isotope substitutions. This dramatic difference of PSIE may serve as an indicator to identify the processes related to the isomerization of alkanes.

Table 5 shows the intermolecular carbon and hydrogen isotope equilibriums between the conformers and isomers of butane. To understand the equilibrium isotope fractionation between *n*-butane and *i*-butane, we need to confirm if it is valid to use the β factor of one conformer to represent that of *n*-butane. In fact, the conformation of *n*-butane does not contain bond break when the internal rotor overcomes a barrier height, therefore cannot affect the isotope signature of *n*-butane. For the equilibrium isotope fractionation between *gauche*-butane and

Table 2
Comparison of harmonic β factors calculated at various computational levels for *trans*-, *gauche*-, and *i*-butane.

T	β factors	*trans*-butane				*gauche*-butane				*i*-butane			
		CCSD(T)	MP2	$MP2^{sf}$	B3LYP	CCSD(T)	MP2	$MP2^{sf}$	B3LYP	CCSD(T)	MP2	$MP2^{sf}$	B3LYP
50 °C	$\beta_1(^{13}C/^{12}C)$	1.1247	1.1269	1.1235	1.1225	1.1245	1.1267	1.1233	1.1223	1.1262	1.1282	1.1248	1.1238
	$\beta_2(^{13}C/^{12}C)$	1.1400	1.1423	1.1383	1.1363	1.1395	1.1419	1.1379	1.1358	1.1528	1.1553	1.1508	1.1470
	β_1(D/H)	9.7293	10.0953	9.5514	9.5839	9.7626	10.1223	9.5763	9.6080	9.6916	10.0346	9.4945	9.5667
	β_2(D/H)	10.3710	10.7536	10.1498	10.2419	10.4029	10.7827	10.1765	10.2792	11.0444	11.4292	10.7645	10.9580
	$\beta(^{13}C/^{12}C)$	1.1323	1.1346	1.1309	1.1294	1.1320	1.1343	1.1306	1.1291	1.1328	1.1350	1.1313	1.1296
	β(D/H)	9.9860	10.3586	9.7908	9.8471	10.0187	10.3865	9.8164	9.8765	9.8269	10.1740	9.6215	9.7058
120 °C	$\beta_1(^{13}C/^{12}C)$	1.0932	1.0949	1.0923	1.0915	1.0931	1.0948	1.0921	1.0914	1.0941	1.0957	1.0930	1.0923
	$\beta_2(^{13}C/^{12}C)$	1.1031	1.1049	1.1018	1.1003	1.1027	1.1045	1.1015	1.0999	1.1114	1.1133	1.1099	1.1071
	β_1(D/H)	5.7586	5.9336	5.6748	5.6885	5.7738	5.9459	5.6863	5.7002	5.7378	5.9021	5.6451	5.6780
	β_2(D/H)	6.0039	6.1825	5.9027	5.9425	6.0173	6.1945	5.9138	5.9587	6.2658	6.4422	6.1409	6.2236
	$\beta(^{13}C/^{12}C)$	1.0982	1.0999	1.0971	1.0959	1.0979	1.0996	1.0968	1.0956	1.0984	1.1001	1.0972	1.0960
	β(D/H)	5.8567	6.0331	5.7659	5.7901	5.8712	6.0454	5.7773	5.8036	5.7906	5.9561	5.6947	5.7325
200 °C	$\beta_1(^{13}C/^{12}C)$	1.0702	1.0715	1.0695	1.0689	1.0701	1.0714	1.0688	1.0688	1.0707	1.0720	1.0699	1.0693
	$\beta_2(^{13}C/^{12}C)$	1.0765	1.0779	1.0756	1.0744	1.0762	1.0776	1.0741	1.0741	1.0818	1.0832	1.0807	1.0785
	β_1(D/H)	3.8615	3.9570	3.8170	3.8232	3.8695	3.9636	3.8297	3.8297	3.8492	3.9390	3.7999	3.8166
	β_2(D/H)	3.9665	4.0623	3.9138	3.9329	3.9730	4.0681	3.9412	3.9412	4.0819	4.1754	4.0182	4.0581
	$\beta(^{13}C/^{12}C)$	1.0734	1.0747	1.0725	1.0717	1.0731	1.0745	1.0714	1.0714	1.0735	1.0748	1.0726	1.0716
	β(D/H)	3.9035	3.9992	3.8557	3.8671	3.9109	4.0054	3.8743	3.8743	3.8724	3.9627	3.8218	3.8408
500 °C	$\beta_1(^{13}C/^{12}C)$	1.0317	1.0324	1.0314	1.0311	1.0316	1.0323	1.0313	1.0310	1.0318	1.0324	1.0314	1.0312
	$\beta_2(^{13}C/^{12}C)$	1.0332	1.0339	1.0328	1.0323	1.0331	1.0337	1.0326	1.0321	1.0344	1.0351	1.0339	1.0330
	β_1(D/H)	1.8931	1.9191	1.8823	1.8829	1.8951	1.9208	1.8839	1.8846	1.8894	1.9140	1.8774	1.8808
	β_2(D/H)	1.9061	1.9315	1.8938	1.8969	1.9076	1.9328	1.8950	1.8989	1.9233	1.9476	1.9089	1.9160
	$\beta(^{13}C/^{12}C)$	1.0324	1.0331	1.0321	1.0317	1.0324	1.0330	1.0320	1.0316	1.0325	1.0331	1.0321	1.0316
	β(D/H)	1.8983	1.9240	1.8869	1.8885	1.9001	1.9256	1.8883	1.8904	1.8928	1.9173	1.8805	1.8843

$MP2^{sf}$ means the harmonic β factors calculated by using scaled harmonic frequencies (scale factor is equal to 0.9816). Subscript 1 or 2 means the non-equivalent positions for isotope substitutions, e.g., β_1(D/H) represents the β factor of hydrogen isotope substitution at the methyl group. $\beta(^{13}C/^{12}C)$ or β(D/H) is the β factor for calculating intermolecular isotope equilibriums.

Table 3
Corrections to the β factors calculated at MP2/6–311+G(d,p) level for *trans*-, *gauche*-, and *i*-butane.

trans-butane		AnZPE	AnEXC	VrZPE	VrEXC	QmCorr	CenDist	HIR	DBOC	*Corr*
50 °C	$\beta_1(^{13}C/^{12}C)$	0.9949	1.0002	0.9999	1.0001	1.0000	1.0000	1.0000	1.1312	1.1258
	$\beta_2(^{13}C/^{12}C)$	0.9948	0.9991	0.9999	1.0001	1.0000	1.0000	1.0000	1.1311	1.1242
	β_1(D/H)	0.9263	1.0015	0.9997	0.9998	1.0000	1.0000	0.9970	1.1396	1.0535
	β_2(D/H)	0.9268	1.0035	0.9996	0.9995	1.0000	1.0000	1.0000	1.1429	1.0620
	$\beta(^{13}C/^{12}C)$	0.9948	0.9997	0.9999	1.0001	1.0000	1.0000	1.0000	1.1312	1.1250
	β(D/H)	0.9265	1.0023	0.9997	0.9997	1.0000	1.0000	0.9982	1.1409	1.0569
120 °C	$\beta_1(^{13}C/^{12}C)$	0.9958	1.0003	0.9999	1.0001	1.0000	1.0000	1.0000	1.1067	1.1024
	$\beta_2(^{13}C/^{12}C)$	0.9957	0.9991	0.9999	1.0001	1.0000	1.0000	1.0000	1.1066	1.1008
	β_1(D/H)	0.9390	1.0017	0.9997	0.9997	1.0000	1.0000	0.9973	1.1134	1.0438
	β_2(D/H)	0.9394	1.0041	0.9996	0.9994	1.0000	1.0000	1.0000	1.1160	1.0516
	$\beta(^{13}C/^{12}C)$	0.9958	0.9997	0.9999	1.0001	1.0000	1.0000	1.0000	1.1066	1.1016
	β(D/H)	0.9392	1.0026	0.9997	0.9996	1.0000	1.0000	0.9984	1.1144	1.0470
200 °C	$\beta_1(^{13}C/^{12}C)$	0.9965	1.0003	0.9999	1.0002	1.0000	1.0000	1.0000	1.0879	1.0845
	$\beta_2(^{13}C/^{12}C)$	0.9964	0.9990	0.9999	1.0002	1.0000	1.0000	1.0000	1.0878	1.0829
	β_1(D/H)	0.9490	1.0018	0.9997	0.9997	1.0000	1.0000	0.9973	1.0933	1.0361
	β_2(D/H)	0.9494	1.0045	0.9996	0.9992	1.0000	1.0000	1.0000	1.0955	1.0436
	$\beta(^{13}C/^{12}C)$	0.9965	0.9997	0.9999	1.0002	1.0000	1.0000	1.0000	1.0878	1.0837
	β(D/H)	0.9492	1.0029	0.9997	0.9995	1.0000	1.0000	0.9984	1.0942	1.0391
500 °C	$\beta_1(^{13}C/^{12}C)$	0.9979	1.0004	0.9999	1.0003	1.0000	1.0000	1.0000	1.0529	1.0513
	$\beta_2(^{13}C/^{12}C)$	0.9978	0.9987	0.9999	1.0003	1.0000	1.0000	1.0000	1.0528	1.0494
	β_1(D/H)	0.9685	1.0020	0.9997	0.9994	1.0000	1.0000	0.9979	1.0561	1.0219
	β_2(D/H)	0.9687	1.0052	0.9996	0.9987	1.0000	1.0000	1.0000	1.0574	1.0279
	$\beta(^{13}C/^{12}C)$	0.9978	0.9995	0.9999	1.0003	1.0000	1.0000	1.0000	1.0529	1.0504
	β(D/H)	0.9686	1.0033	0.9997	0.9991	1.0000	1.0000	0.9988	1.0566	1.0243

gauche-butane		AnZPE	AnEXC	VrZPE	VrEXC	QmCorr	CenDist	HIR	DBOC	*Corr*
50 °C	$\beta_1(^{13}C/^{12}C)$	0.9950	0.9996	1.0000	1.0001	1.0000	1.0000	1.0000	1.1312	1.1253
	$\beta_2(^{13}C/^{12}C)$	0.9944	0.9992	0.9997	0.9998	1.0000	1.0000	1.0000	1.1311	1.1234
	β_1(D/H)	0.9242	1.0005	0.9998	1.0005	1.0000	1.0001	0.9970	1.1395	1.0508
	β_2(D/H)	0.9256	1.0014	0.9996	1.0000	1.0000	0.9999	1.0001	1.1428	1.0588
	$\beta(^{13}C/^{12}C)$	0.9947	0.9994	0.9999	1.0000	1.0000	1.0000	1.0000	1.1312	1.1243
	β(D/H)	0.9248	1.0008	0.9997	1.0003	1.0000	1.0000	0.9982	1.1408	1.0540
120 °C	$\beta_1(^{13}C/^{12}C)$	0.9959	0.9996	1.0000	1.0002	1.0000	1.0001	1.0000	1.1067	1.1019
	$\beta_2(^{13}C/^{12}C)$	0.9954	0.9993	0.9997	0.9998	1.0000	1.0000	1.0000	1.1066	1.1001
	β_1(D/H)	0.9373	1.0002	0.9998	1.0006	1.0000	1.0001	0.9975	1.1133	1.0416
	β_2(D/H)	0.9385	1.0017	0.9996	1.0000	1.0000	0.9998	1.0002	1.1160	1.0487
	$\beta(^{13}C/^{12}C)$	0.9956	0.9994	0.9999	1.0000	1.0000	1.0000	1.0000	1.1066	1.1010
	β(D/H)	0.9378	1.0008	0.9997	1.0003	1.0000	1.0000	0.9986	1.1144	1.0444
200 °C	$\beta_1(^{13}C/^{12}C)$	0.9966	0.9996	1.0000	1.0002	1.0000	1.0001	1.0000	1.0879	1.0840
	$\beta_2(^{13}C/^{12}C)$	0.9962	0.9993	0.9997	0.9997	1.0000	1.0000	1.0000	1.0878	1.0823
	β_1(D/H)	0.9476	0.9999	0.9998	1.0007	1.0000	1.0001	0.9979	1.0933	1.0343
	β_2(D/H)	0.9486	1.0019	0.9996	1.0000	1.0000	0.9998	1.0004	1.0954	1.0409
	$\beta(^{13}C/^{12}C)$	0.9964	0.9995	0.9999	1.0000	1.0000	1.0000	1.0000	1.0878	1.0832
	β(D/H)	0.9480	1.0007	0.9997	1.0004	1.0000	1.0000	0.9989	1.0942	1.0369
500 °C	$\beta_1(^{13}C/^{12}C)$	0.9979	0.9996	1.0000	1.0004	1.0000	1.0001	1.0003	1.0529	1.0510
	$\beta_2(^{13}C/^{12}C)$	0.9977	0.9995	0.9997	0.9996	1.0000	0.9999	1.0003	1.0528	1.0493
	β_1(D/H)	0.9676	0.9989	0.9998	1.0011	1.0000	1.0001	0.9988	1.0561	1.0207
	β_2(D/H)	0.9682	1.0021	0.9996	0.9999	1.0000	0.9997	1.0011	1.0574	1.0263
	$\beta(^{13}C/^{12}C)$	0.9978	0.9995	0.9999	1.0000	1.0000	1.0000	1.0003	1.0529	1.0502
	β(D/H)	0.9679	1.0002	0.9997	1.0006	1.0000	0.9999	0.9997	1.0566	1.0229

i-butane		AnZPE	AnEXC	VrZPE	VrEXC	QmCorr	CenDist	HIR	DBOC	*Corr*
50 °C	$\beta_1(^{13}C/^{12}C)$	0.9947	1.0000	0.9999	1.0001	1.0000	1.0000	1.0000	1.1313	1.1253
	$\beta_2(^{13}C/^{12}C)$	0.9950	0.9995	0.9999	1.0000	1.0000	1.0000	1.0000	1.1310	1.1246
	β_1(D/H)	0.9287	1.0017	0.9997	1.0002	1.0000	1.0000	0.9972	1.1393	1.0568
	β_2(D/H)	0.9284	1.0046	1.0000	1.0000	1.0000	0.9999	1.0000	1.1451	1.0678
	$\beta(^{13}C/^{12}C)$	0.9947	0.9999	0.9999	1.0001	1.0000	1.0000	1.0000	1.1312	1.1251
	β(D/H)	0.9287	1.0020	0.9997	1.0002	1.0000	1.0000	0.9975	1.1399	1.0579
120 °C	$\beta_1(^{13}C/^{12}C)$	0.9956	1.0001	0.9999	1.0002	1.0000	1.0000	1.0000	1.1067	1.1020
	$\beta_2(^{13}C/^{12}C)$	0.9959	0.9996	0.9999	1.0000	1.0000	1.0000	1.0000	1.1065	1.1013
	β_1(D/H)	0.9410	1.0022	0.9997	1.0003	1.0000	1.0000	0.9985	1.1132	1.0482
	β_2(D/H)	0.9407	1.0053	1.0000	1.0000	1.0000	0.9999	1.0000	1.1178	1.0570
	$\beta(^{13}C/^{12}C)$	0.9957	1.0000	0.9999	1.0001	1.0000	1.0000	1.0000	1.1066	1.1018
	β(D/H)	0.9410	1.0025	0.9997	1.0002	1.0000	1.0000	0.9987	1.1137	1.0491
200 °C	$\beta_1(^{13}C/^{12}C)$	0.9964	1.0001	0.9999	1.0002	1.0000	1.0000	1.0000	1.0879	1.0842
	$\beta_2(^{13}C/^{12}C)$	0.9966	0.9997	0.9999	1.0000	1.0000	1.0000	1.0000	1.0877	1.0834
	β_1(D/H)	0.9508	1.0026	0.9997	1.0003	1.0000	1.0000	0.9995	1.0932	1.0416
	β_2(D/H)	0.9505	1.0058	1.0000	1.0000	1.0000	0.9999	1.0000	1.0970	1.0485
	$\beta(^{13}C/^{12}C)$	0.9964	1.0000	0.9999	1.0001	1.0000	1.0000	1.0000	1.0878	1.0840
	β(D/H)	0.9507	1.0029	0.9997	1.0003	1.0000	1.0000	0.9996	1.0936	1.0423

(*continued on next page*)

Table 3 (*continued*)

i-butane		AnZPE	AnEXC	VrZPE	VrEXC	QmCorr	CenDist	HIR	DBOC	*Corr*
50 °C	$\beta_1(^{13}C/^{12}C)$	0.9947	1.0000	0.9999	1.0001	1.0000	1.0000	1.0000	1.1313	1.1253
500 °C	$\beta_1(^{13}C/^{12}C)$	0.9978	1.0002	0.9999	1.0003	1.0000	1.0000	1.0000	1.0529	1.0511
	$\beta_2(^{13}C/^{12}C)$	0.9979	0.9998	0.9999	1.0000	1.0000	1.0000	1.0000	1.0528	1.0502
	β_1(D/H)	0.9696	1.0034	0.9997	1.0005	1.0000	1.0000	1.0019	1.0560	1.0295
	β_2(D/H)	0.9694	1.0064	1.0000	0.9999	1.0000	0.9998	1.0000	1.0583	1.0321
	$\beta(^{13}C/^{12}C)$	0.9978	1.0001	0.9999	1.0003	1.0000	1.0000	1.0000	1.0529	1.0509
	β(D/H)	0.9696	1.0037	0.9997	1.0004	1.0000	1.0000	1.0017	1.0563	1.0298

AnZPE is the anharmonic correction for the zero-point energy. **AnEXC** is the anharmonic correction for the vibrational excited states. **VrZPE** is the vibration-rotation coupling correction for the zero-point energy. **VrEXC** is the vibration-rotation coupling correction for the vibrational excited states. **QmCorr** is a correction for quantum mechanical rotation. **CenDist** is the centrifugal distortion correction arising from rotation-vibration interaction. **HIR** is the correction due to hindered internal rotations. **DBOC** is the diagonal Born-Oppenheimer correction. ***Corr*** means the overall contribution of the corrections considered here, which is equal to **AnZPE · AnEXC · VrZPE · VrEXC · QmCorr · CenDist · HIR · DBOC**.

trans-butane, our results show that the conformers of *n*-butane contain similar isotope signature when they reach isotope equilibriums. Therefore, it is reasonable to use the β factors of *trans*-butane to represent the β factors of *n*-butane under currently experimental precisions (e.g., within ± 0.5‰ and ± 5‰ for $\delta^{13}C$ and δD values, Liu et al., 2019). Considering the similar finding for PSIE, we will use the isotope signatures of *trans*-butane to represent those of *n*-butane hereafter. As shown in Table 5, there are negligible carbon isotope fractionations between *n*-butane and *i*-butane when they reach equilibriums. However, equilibrium hydrogen isotope fractionations show that *n*-butane is enriched in deuterium than *i*-butane at equilibriums. Within the temperature range of 200 °C to 500 °C, a crossover of hydrogen isotope fractionation was found when we calculate the equilibrium isotope effects beyond the harmonic and Born-Oppenheimer approximation.

4. Discussion

4.1. Uncertainties in α values

The accuracy of calculated α values mainly depends on the accuracy of harmonic frequencies, which is further determined by the chosen theoretical methods and basis sets. According to our computational experience, the influence of theoretical methods is stronger than that of basis sets. When the utilized basis sets are sufficient in modeling, α values calculated from different basis sets should be very close to each other under the same theoretical method. For example, the equilibrium isotope fractionation factors calculated from 6–311+G(d,p) and aug–cc–pVTZ are almost the same under MP2 or B3LYP method. This means 6–311+G(d,p) basis set is adequate for the content of this study.

On the harmonic approximation, we used a frequency scale factor to correct the overestimation of harmonic frequencies generated from MP2/6–311+G(d,p). By comparing the α values of MP2 with and without frequency scaling, we can conclude that the use of scale factor only has limited influence on our calculations. Meanwhile, the difference between α values of MP2 and $MP2^{sf}$ can be considered as the computational errors due to the incomplete treatment of electron correlation and the use of finite basis sets. This suggests the computational error of α values obtained from CCSD(T)/6–311+G(d,p) should be even smaller than the deviation between α(MP2) and $\alpha(MP2^{sf})$ values. The precision of our harmonic predications at CCSD(T)/6–311+G(d,p) therefore can be roughly estimated to be within ± 1‰ for $1000\ln\alpha_{2\text{–}1}(^{13}C/^{12}C)$, ± 6‰ for $1000\ln\alpha_{2\text{–}1}$(D/H), and ± 1‰ for $1000\ln\alpha$(D/H), which is comparable to the magnitudes of experimental precisions (Liu et al., 2019; Julien et al., 2020).

Among all the corrections, anharmonicity plays an important role to improve the accuracy of α values for both carbon and hydrogen isotope substitutions. Even so, the magnitude that anharmonicity contributes to α values is about the same as the computational error of our harmonic predictions. Notably, HIR and DBOC together contribute more than half of the total correction (*Corr*) for hydrogen isotope substitutions, but little for carbon isotope substitutions. The significance of HIR in this study can be attributed to its "position-specific" characteristic, i.e., HIR shows its only influence on the hydrogen isotope substitutions in the methyl groups of butane. Unlike the effects of anharmonicity, the importance of HIR is enlarged in the calculation of α values although the contribution of HIR to β values is much less than that of anharmonicity. DBOC is a small effect on electronic energy that is neglected in the Born-Oppenheimer approximation. The magnitude of this effect is argued to be $\sim Z^2/M$, where Z means atomic number, and M means nuclear mass (Handy et al., 1986; Imafuku et al., 2016). Therefore, consideration of DBOC is expected to improve the accuracy of isotope fractionation calculations for light elements, especially H/D exchanges (Zhang and Liu, 2018). As shown in Liu and Liu (2016), the numerical uncertainty of higher-order energy terms does not need to consider in the calculation of isotope effects because some of the errors should be canceled. For example, the contributions of DBOC to α values calculated from CCSD/aug–cc–pVTZ and MP2/6–311+G(d,p) are almost identical (i.e., with the deviation of ~ 0.1‰ for correcting $1000\ln\alpha_{2\text{–}1}$(D/H) in *trans*-butane at 50 °C). However, the methodology uncertainty of HIR is hard to estimate. Further comparison between theoretical calculation and experimental observation of isotope effects may provide valuable information to evaluate the uncertainty of HIR.

Meanwhile, we found that the harmonic results α(B3LYP) are very close to our best estimated α values, $\alpha(CCSD(T)^{Corr})$. Because the calculations under CCSD(T) method are quite time-consuming, it is unrealistic to use CCSD(T) method for larger molecules. Obviously, B3LYP method provides a better balance of computational cost and overall reliability for the calculation of harmonic frequencies (Byrd et al., 2001). Therefore, a compromise for larger molecules can be obtained for isotope fractionation factors at the harmonic approximation under DFT method (e.g., B3LYP), which should meet the needs of many theoretical studies (Wang et al., 2009a,b; He et al., 2020).

4.2. Temperature dependences

The intramolecular and intermolecular isotope fractionation factors at equilibriums were fitted as the fifth-order polynomial expressions of 1000/T in Table 6. Because there is no measurable equilibrium carbon isotope fractionation between *n*-butane and *i*-butane, we did not show the polynomial fit for the carbon isotope equilibriums. We selected 55 points within the temperature range from 0 °C to 726.85 °C to fit the fifth-order polynomials for the harmonic predictions (CCSD(T)). Results of 6 temperature points (0 °C, 50 °C, 120 °C, 200 °C, 500 °C, 726.85 °C) were used for fitting the contribution of higher-order corrections (*Corr*). The polynomials of $CCSD(T)^{Corr}$ then is equal to the combination of the fifth-order polynomial expressions of CCSD(T) and *Corr*. Note that the polynomial fits are only available during the fitted temperature range. There is no intercept in our polynomial fits because $1000\ln\alpha$ values theoretically become 0 when temperature is extremely high. The fitted $1000\ln\alpha$ values are generally within 0.04‰ compared to our original data for intramolecular hydrogen isotope equilibriums, within 0.02‰ for intramolecular carbon isotope equilibriums, within 0.004‰ for

Table 4
Intramolecular isotope effects at equilibriums predicted at various computational levels for *trans*-, *gauche*-, and *i*-butane.

T	intramolecular	*trans*-butane						*gauche*-butane						*i*-butane					
	isotope equilibriums	CCSD(T)	MP2	$MP2^{sf}$	B3LYP	*Corr*	$CCSD(T)^{Corr}$	CCSD(T)	MP2	$MP2^{sf}$	B3LYP	*Corr*	$CCSD(T)^{Corr}$	CCSD(T)	MP2	$MP2^{sf}$	B3LYP	*Corr*	$CCSD(T)^{Corr}$
50 °C	$1000\ln\alpha_{2-1}(^{13}C/^{12}C)$	13.4	13.6	13.1	12.2	−1.3	**12.1**	13.2	13.4	12.9	11.9	−1.7	**11.5**	23.4	23.7	22.9	20.4	−0.6	**22.7**
	$1000\ln\alpha_{2-1}(D/H)$	63.9	63.2	60.8	66.4	8.1	**72.0**	63.5	63.2	60.8	67.5	7.5	**71.1**	130.7	130.1	125.5	135.8	10.3	**141.0**
120 °C	$1000\ln\alpha_{2-1}(^{13}C/^{12}C)$	9.0	9.1	8.7	8.0	−1.4	**7.6**	8.8	8.9	8.5	7.8	−1.6	**7.1**	15.7	16.0	15.3	13.4	−0.7	**15.0**
	$1000\ln\alpha_{2-1}(D/H)$	41.7	41.1	39.4	43.7	7.4	**49.2**	41.3	41.0	39.2	44.3	6.8	**48.1**	88.0	87.6	84.2	91.8	8.3	**96.3**
200 °C	$1000\ln\alpha_{2-1}(^{13}C/^{12}C)$	5.9	5.9	5.7	5.1	−1.5	**4.4**	5.7	5.7	5.5	4.9	−1.6	**4.1**	10.3	10.5	10.0	8.5	−0.7	**9.6**
	$1000\ln\alpha_{2-1}(D/H)$	26.8	26.3	25.1	28.3	7.2	**34.0**	26.4	26.0	24.8	28.7	6.3	**32.7**	58.7	58.3	55.9	61.3	6.6	**65.3**
500 °C	$1000\ln\alpha_{2-1}(^{13}C/^{12}C)$	1.5	1.5	1.4	1.1	−1.7	**−0.3**	1.4	1.4	1.3	1.0	−1.6	**−0.2**	2.6	2.6	2.4	1.7	−0.8	**1.7**
	$1000\ln\alpha_{2-1}(D/H)$	6.9	6.5	6.1	7.4	5.9	**12.7**	6.6	6.2	5.9	7.5	5.4	**12.0**	17.8	17.4	16.6	18.5	2.5	**20.3**

The results of CCSD(T), MP2 and B3LYP are isotope equilibriums calculated on the harmonic approximation without frequency scaling. $MP2^{sf}$ means the results calculated on a frequency-scaled MP2/6–311+G(d,p) model. *Corr* means the contribution of all the higher-order corrections. $CCSD(T)^{Corr}$ means the harmonic results of CCSD(T) combined with the contribution of corrections.

intermolecular hydrogen isotope equilibriums.

We plot the temperature dependences of $1000\ln\alpha$ values with and without corrections in Fig. 2, comparing with the results of Polyakov and Horita (2021) for carbon isotope equilibriums and Wang et al. (2009a) for hydrogen isotope equilibriums. Note that the results of Wang et al. (2009a) were calculated under the treatment of "cutoff" effects and were fitted for the temperature range from 0 °C to 100 °C. At low temperature, our $1000\ln\alpha$ values show nearly linear correlation against 1000/T but have roughly linear correlation with T^{-1} at high temperature. For both position-specific carbon and hydrogen isotope effects, the equilibrium isotope fractionations in *i*-butane are almost twice the magnitude of isotope fractionations in *n*-butane. This isotopic characteristic may have potential applications, e.g., identifying isotope signatures inherited from branched alkanes or isomerization of chain alkanes. For equilibrium isotope fractionation between *i*-butane and *n*-butane, only the temperature dependence of hydrogen isotope fractionations is detectable.

For the intramolecular carbon isotope effects (Fig. 2A), our results are generally in agreement with the calculation of Polyakov and Horita (2021) although deviations of ~ 2‰ can be found between our results of $CCSD(T)^{Corr}$ and those of Polyakov and Horita (2021). For the intramolecular hydrogen isotope effects (Fig. 2B), our results show different temperature dependences from those of Wang et al. (2009a), which suggests that the calculation of equilibrium isotope fractionations using "cutoff" treatment is not accurate enough for the study of smaller hydrocarbons like butane. For isotope fractionations between *n*-butane and *i*-butane (Fig. 2C), there are significant differences between our results and those of Polyakov and Horita (2021) and Wang et al. (2009a). In contrast to our findings, for example, Polyakov and Horita (2021) predicted *n*-butane should be enriched in ^{13}C relative to *i*-butane in a measureable magnitude when they reach isotope equilibriums. We note that our calculation of equilibrium carbon isotope fractionation factors between butane isomers are in agreement with those of Thiagarajan et al. (2020). Since it is difficult to separate *i*-butane from *n*-butane in measurements (Thiagarajan et al., 2020), our results would provide valuable information for the experimental observations.

Fig. 3 shows the relationships of $1000\ln\alpha_{2-1}$ for intramolecular isotope equilibriums in *n*-butane and *i*-butane. From a linear fitting point of view, the slopes of the equilibrium models are about 5 for *n*-butane and slightly larger than 5 for *i*-butane on the harmonic approximation. If the contribution of higher-order energy terms is considered, the slopes in Fig. 3 should be a little larger (~ 6) for both *n*-butane and *i*-butane. We found the slopes are smaller than the slope for intramolecular isotope equilibriums in propane (i.e., ~ 7.5, Webb and Miller III, 2014). Since evidence shows that the intramolecular isotope signatures in propane are getting closer to equilibrium distributions with the increase of maturity (Liu et al., 2019), these curves may sever as an anchor to identify stages of maturation for oil and gas reservoirs.

Table 7 presents temperature-dependent abundance ratios of butane conformers and isomers when the species reach equilibriums. The free energy differences we calculated at CCSD(T)/6–311+G(d,p) and MP2/6–311+G(d,p) are consistent with the previous studies (e.g., Karton et al., 2009; Barna et al., 2012), but B3LYP/6–311+G(d,p) failed to generate reasonable energy differences between *n*-butane and *i*-butane. It was reported that B3LYP sometimes may perform worse than HF methods for calculating energy differences (Zhao and Truhlar, 2008). Although the performance of B3LYP is good for harmonic frequency calculations, comparisons with other methods like MP2 or M06 suite are necessary if relative energies are required accurately. At equilibriums, the abundance sequence of butane should be *i*-butane ≫ *trans*-butane > *gauche*-butane. During the temperature range of interest, the abundance of *trans*-butane accounts for ~ 70% of *n*-butane, and collisions between molecules can provide enough energies to make the internal rotation mode overcome the barrier height without bond breading (Cormanich and Freitas, 2009). In natural settings, the concentration of *n*-butane is usually observed to be similar to or even larger than that of *i*-butane (e.g., Liu et al., 2019; Suda et al., 2017), which means the proportions of

Table 5
Intermolecular isotope fractionations at equilibriums between butane isomers calculated at various computational levels.

butane		*gauche-trans*						*trans-iso*					
T	1000lnα	CCSD(T)	MP2	MP2^{sf}	B3LYP	*Corr*	CCSD(T)^{Corr}	CCSD(T)	MP2	MP2^{sf}	B3LYP	*Corr*	CCSD(T)^{Corr}
50 °C	$^{13}C/^{12}C$	−0.3	−0.3	−0.3	−0.3	−0.6	**−0.9**	−0.4	−0.4	−0.3	−0.2	−0.1	**−0.5**
	D/H	3.3	2.7	2.6	3.0	−2.7	**0.6**	16.1	18.0	17.4	14.5	−1.0	**15.1**
120 °C	$^{13}C/^{12}C$	−0.3	−0.2	−0.2	−0.2	−0.5	**−0.8**	−0.2	−0.2	−0.2	0.0	−0.2	**−0.4**
	D/H	2.5	2.0	2.0	2.3	−2.4	**0.0**	11.3	12.9	12.4	10.0	−2.0	**9.3**
200 °C	$^{13}C/^{12}C$	−0.2	−0.2	−0.2	−0.2	−0.5	**−0.7**	−0.1	−0.1	−0.1	0.0	−0.3	**−0.4**
	D/H	1.9	1.6	1.5	1.9	−2.0	**−0.1**	8.0	9.2	8.8	6.8	−3.1	**4.9**
500 °C	$^{13}C/^{12}C$	−0.1	−0.1	−0.1	−0.1	−0.2	**−0.3**	0.0	0.0	0.0	0.0	−0.5	**−0.5**
	D/H	0.9	0.8	0.8	1.0	−1.4	**−0.4**	2.9	3.5	3.4	2.2	−5.3	**−2.4**

Table 6
Fifth-order polynomial fits of intramolecular and intermolecular isotope fractionation factors at equilibriums from 273.15 K to 1000 K.

273.15 K - 1000 K			A	B	C	D	E
CCSD(T)	*n*-butane	1000lnα_{2-1}($^{13}C/^{12}C$)	0.04606	−0.49203	1.64241	−0.19996	−0.41041
		1000lnα_{2-1}(D/H)	0.15997	−1.86117	6.97651	−1.61143	−0.69740
	i-butane	1000lnα_{2-1}($^{13}C/^{12}C$)	0.08818	−0.92497	3.01062	−0.36977	−0.81215
		1000lnα_{2-1}(D/H)	0.27231	−3.14150	11.22596	1.01955	−0.30995
	n-i	1000lnα(D/H)	0.01842	−0.19850	0.52517	1.44545	−0.11692
Corr	*n*-butane	1000lnα_{2-1}($^{13}C/^{12}C$)	−0.13750	1.37277	−5.21050	9.21319	−7.12072
		1000lnα_{2-1}(D/H)	0.04985	−0.55541	2.58028	−6.42032	9.64809
	i-butane	1000lnα_{2-1}($^{13}C/^{12}C$)	−0.04905	0.53921	−2.21285	4.15372	−3.35020
		1000lnα_{2-1}(D/H)	0.11318	−0.96804	2.41149	−0.66176	0.59192
	n-i	1000lnα(D/H)	−0.06270	0.80249	−4.50287	12.69125	−14.51647
CCSD(T)^{Corr}	*n*-butane	1000lnα_{2-1}($^{13}C/^{12}C$)	−0.09144	0.88074	−3.56809	9.01323	−7.53113
		1000lnα_{2-1}(D/H)	0.20982	−2.41658	9.55679	−8.03175	8.95069
	i-butane	1000lnα_{2-1}($^{13}C/^{12}C$)	0.03913	−0.38576	0.79777	3.78395	−4.16235
		1000lnα_{2-1}(D/H)	0.38549	−4.10954	13.63745	0.35779	0.28197
	n-i	1000lnα(D/H)	−0.04428	0.60399	−3.97770	14.13670	−14.63339

Polynomial fit follows the form: $1000ln\alpha = A\left(\frac{1000}{T}\right)^5 + B\left(\frac{1000}{T}\right)^4 + C\left(\frac{1000}{T}\right)^3 + D\left(\frac{1000}{T}\right)^2 + E\left(\frac{1000}{T}\right)$.

CCSD(T)^{Corr} = CCSD(T) + *Corr*.

butane isomers do not reach the equilibrated scenario. Because the dissociation energy of *n*-butane and *i*-butane is similar, it suggests that the proportion may be controlled by precursor hydrocarbons and formation mechanisms. For example, both *n*-butane and *i*-butane undergo C—C bond cracking processes during the formation of thermogenic gas. This also implies that methane, ethane, and propane should inherit partial isotope signatures from precursor butane, and the position-specific carbon isotope effects in butane may not be able to serve as a geothermometer. Recently, Thiagarajan et al. (2020) found that the bulk carbon and hydrogen isotope compositions of ethane, propane, *n*-butane and *n*-pentane approach equilibriums as the maturity increases for most studied gas reservoirs, but *i*-butane and *i*-pentane do not show isotope equilibrated pattern. It may be also possible that *i*-alkanes form in a different pattern from that of *n*-alkanes. Therefore, the isotopic distributions combined with the proportions of butane isomers may provide a clue to the formation mechanism of *i*-alkanes.

4.3. Geochemical applications

4.3.1. Hydrogen isotope geothermometry

Although the δD values in *n*-alkyl and isoprenoid carbon skeletons suggest hydrogen barely exchanges in the young, cool sediments (Andersen et al., 2001; Yang and Huang, 2003), similar measurements show strong evidence of hydrogen exchange process in many ancient rocks (Sessions et al., 2004). Experimental estimates of exchange rates between organic hydrogen and water also suggest that hydrogen exchanges can occur on a geological timescale of 10^4–10^8 years at warm conditions (Sessions et al., 2004). The experimental lifetimes of hydrogen exchanges between propane and water are only in the order of days in the present of Ni and Pd at 200 °C, and metal catalytic reactions showed that intramolecular hydrogen isotope equilibriums of propane can be faster achieved in anhydrous environments than in hydrous environments (Xie et al., 2018). The isotopic measurements of natural samples suggest that terminal H of propane may equilibrate with water from the beginning, and the intramolecular hydrogen isotope signatures of propane with the highest maturity in Woodford shale may reflect isotope equilibrated distributions (Liu et al., 2019). Under hydrothermal conditions, experimental observations suggested that short chain *n*-alkanes and *n*-alkenes can achieve redox-dependent metastable equilibriums rapidly (Seewald, 1994, 2001, 2003), *n*-butane and *n*-butene are likely approaching isotopic equilibriums driven by reversible hydrogen isotope exchanges with water (Reeves et al., 2012). Based on a pseudo first-order approximation, hydrogen exchange half-times ($t_{1/2}$) were hypothetically estimated to be 1000 years and 10,000 years for methylene and methyl H positions and averaged 6400 years for all H positions in *n*-butane (Sessions et al., 2004). These evidences suggest that intramolecular and intermolecular hydrogen isotope equilibriums within and between butane isomers may serve as a promising geothermometer for natural settings.

4.3.2. Aerobic and anaerobic microbial oxidations

Microorganisms are capable to oxidize hydrocarbons aerobically or anaerobically (Atlas, 1995; Kniemeyer et al., 2007). Understanding the isotope fractionations associated with aerobic and anaerobic microbial oxidization of hydrocarbons would provide information to identify the source and sink of hydrocarbons. Kinnaman et al. (2007) observed the $\delta^{13}C$ and δD variations associated with the aerobic microbial oxidation of methane, ethane, propane, and *n*-butane, e.g., the $\delta^{13}C$ values of resident *n*-butane changed from −30.8‰ to −18.3‰ in the aerobic microbial oxidation experiment at 15 °C, yielding a carbon isotope fractionation factor of −2.9‰ ± 0.9 for a Rayleigh fractionation model. The fractionation factors can be applied to determine oxidation of

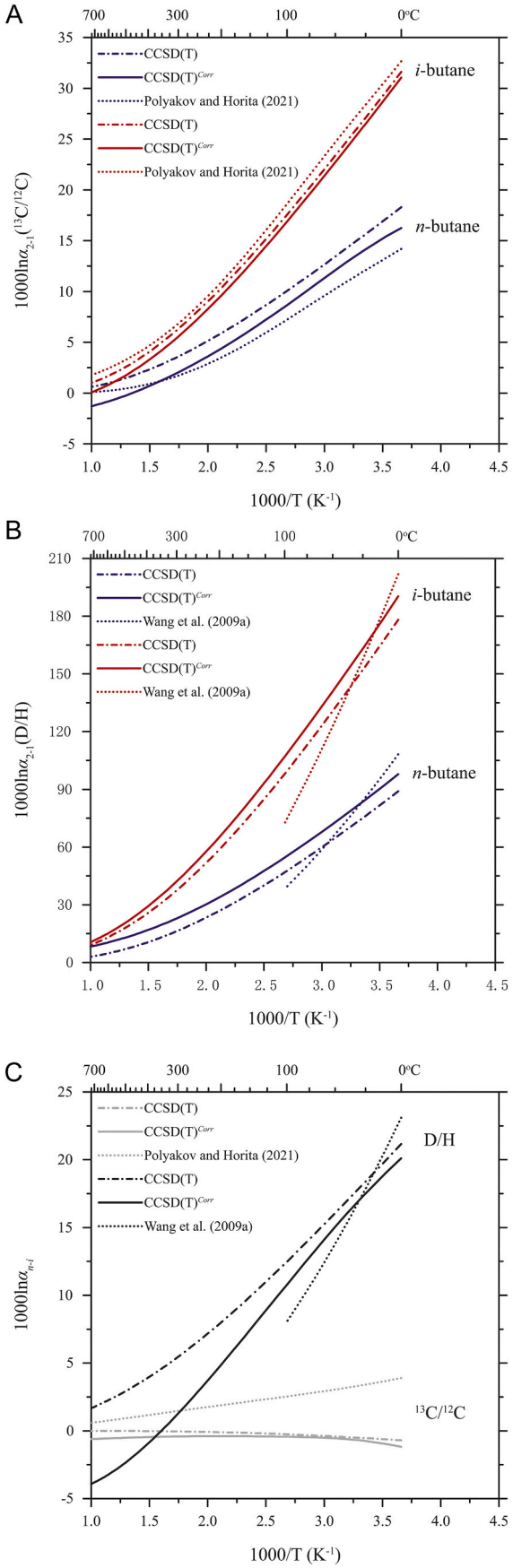

Fig. 2. Equilibrium isotope fractionation factors (1000lnα) within and between butane isomers.

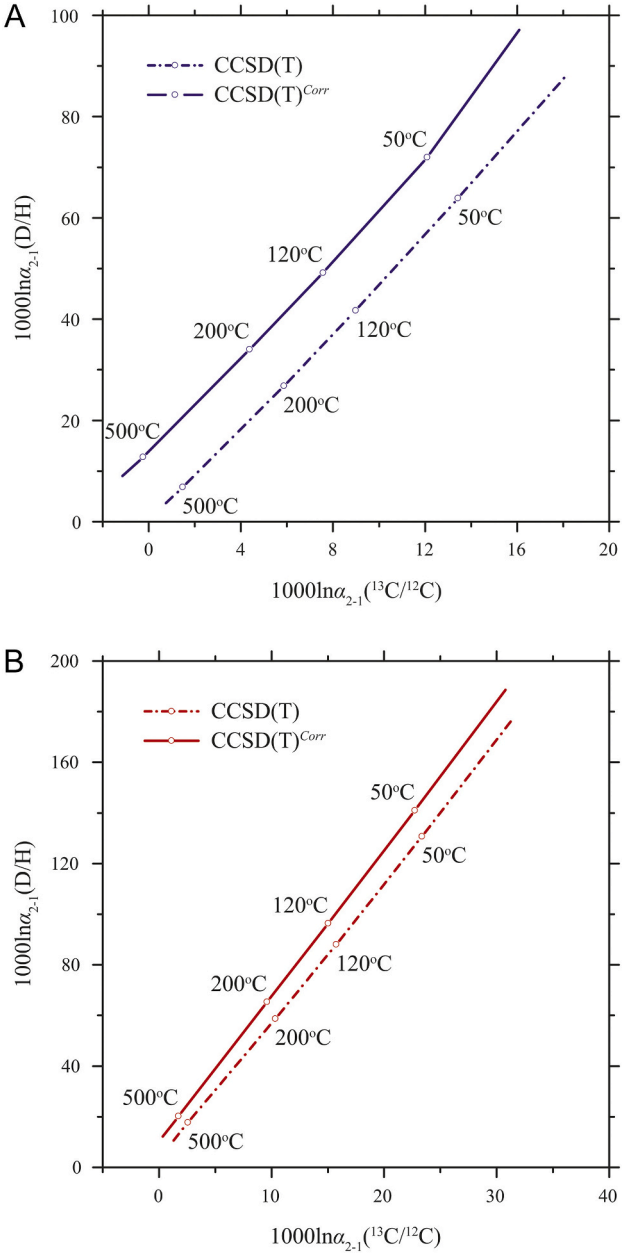

Fig. 3. Equilibrium models of intramolecular isotope effects in (A) *n*-butane and (Bb) *i*-butane.

hydrocarbons in the oxic marine sediments at 15 °C. Gilbert et al. (2019) applied position-specific carbon isotope effects of propane to trace processes related to anaerobic microbial oxidation of hydrocarbons. This isotope analysis may further provide insights into understand the mechanisms of biochemical processes that change the intramolecular isotope signatures of hydrocarbons.

Aerobic and anaerobic consumptions of butane invoke C—H or C—C bond breaking processes, therefore could change intramolecular carbon/hydrogen isotope signatures dramatically from the equilibrium isotope fractionations. For example, a novel oxidation mechanism of butane is observed in the presence of the archaeal genus, *Candidatus Syntrophoarchaeum* (Singh et al., 2017). The introduction of position-specific carbon/hydrogen isotope analysis of butane would expose correlated information to track biogeochemical cycle of hydrocarbons. We expect that the intramolecular isotope equilibrium signatures of butane may serve as a reference frame for identifying kinetic processes like aerobic and anaerobic microbial oxidations of hydrocarbons.

Table 7
Equilibrated abundance ratios of butane conformers and isomers at various temperatures.

Conformer	$\Delta E_{gauche\text{-}trans}$ (J mol^{-1})[a]			$R_{trans/gauche}$[b]		
T	CCSD(T)	MP2	B3LYP	CCSD(T)	MP2	B3LYP
50 °C	2993	2809	3781	3.0	2.8	4.1
120 °C	3103	2909	3815	2.6	2.4	3.2
200 °C	3235	3030	3854	2.3	2.2	2.7
500 °C	3731	3492	4001	1.8	1.7	1.9

Isomer	$\Delta E_{n\text{-}i}$ (J mol^{-1})[a]			$R_{i/n}$[c]		
T	CCSD(T)	MP2	B3LYP	CCSD(T)	MP2	B3LYP
50 °C	7175	7535	1468	14.4	16.5	1.7
120 °C	6881	7021	964	8.2	8.6	1.3
200 °C	6574	6461	420	5.3	5.2	1.1
500 °C	5611	4555	−1420	2.4	2.0	0.8

[a] Free energy differences between butane conformers/isomers obtained from Gaussian 09 package.
[b] Abundance ratios (R) at equilibriums calculated using free energy values according to $\Delta G = -RT\ln K$.
[c] Here the free energy values of *trans*-butane are used to represent the values of *n*-butane.

4.3.3. Abiotic origin of hydrocarbons

Recently, Suda et al. (2017) found the relationship of $\delta^{13}C$ values of C_1 to C_5 straight-chain alkanes sampled from Hakuba Happo hot springs (Japan) is consistent with an abiotic polymerization model. Both bulk and position-specific isotope signatures provide valuable information for interpreting the mechanism of abiotic synthesis. In Suda et al. (2017), an unusual isotopic enrichment in *i*-butane was found to be 5–8‰ enriched in $\delta^{13}C$ relative to *n*-butane. Therefore, it is promising that the position-specific carbon and hydrogen isotope effects in butane can provide additional information for understanding formation mechanisms of abiotic hydrocarbons. Meanwhile, calibrations are thought to be needed for constraining the accuracy of position-specific isotope analysis when the analysis is applied to natural samples. The equilibrium properties calculated theoretically then may serve as a calibration of experimental analyses. Moreover, abiotic hydrocarbons can be produced during formation and evolution processes of planets and their satellites. For example, computational simulations show that the abundance of butane may be similar to that of propane in Titan's atmosphere (Dobrijevic et al., 2016). It may be possible that extraterrestrial hydrocarbons form in a thermodynamic pattern. The intramolecular isotope equilibriums in butane may further provide unique information for understanding formations of extraterrestrial hydrocarbons.

5. Conclusions

Accurate temperature dependences of intramolecular and intermolecular carbon and hydrogen isotope distributions at equilibriums within and between butane isomers have been calculated beyond the harmonic approximation and the Born-Oppenheimer approximation. $1000\ln\alpha_{2\text{–}1}$ values in *i*-butane are found to be almost twice the values in *n*-butane for both carbon and hydrogen isotope equilibriums. The contribution of higher-order energy terms is found to be comparable to the magnitude of the current experimental measurements, e.g., at 200 °C, the total contribution of corrections is −1.5‰ and +7‰ to $1000\ln\alpha_{2\text{–}1}$ values for intramolecular carbon and hydrogen isotope equilibriums in *n*-butane, −0.3‰ and −3.1‰ to $1000\ln\alpha$ values for equilibrium carbon and hydrogen isotope fractionations between *n*-butane and *i*-butane. Our results show that anharmonicity plays an important role to improve the accuracy of α values for both carbon and hydrogen isotope equilibriums. Along with anharmonicity, hindered internal rotation and diagonal Born-Oppenheimer correction contribute significantly for accurate predictions of position-specific hydrogen isotope equilibriums. The proportions of equilibrated butane conformers and isomers are calculated for typical temperature points, and the abundance sequence follows *i*-butane ≫ *trans*-butane > *gauche*-butane. The DFT method B3LYP is evaluated as a practical option to produce isotope fractionation factors for larger molecules, but may fail to generate reasonable proportions of equilibrated species. Our predictions provide a theoretical framework for further studies of position-specific isotope effects in butane, such as calibrating experimental measurements, establishing thermometers, and recognizing kinetic processes.

Declaration of Competing Interest

The authors declare that they have no known competing financial interests or personal relationships that could have appeared to influence the work reported in this paper.

Acknowledgments

Q.L. and Y.L. are grateful for the funding support from the Strategic Priority Research Program of Chinese Academy of Sciences (XDB 41000000, XDB18010100), National Natural Science Foundation of China (41473026, 41530210). Y.L. is grateful for funding support from pre-research Project on Civil Aerospace Technologies No. D 020202 funded by Chinese National Space Administration. X.Y. is grateful for the funding support from National Natural Science Foundation of China (41603015). N.Y. is grateful for the Japan Society for the Promotion of Science KAKENHI Grant-in-aid, JP17H06105, under the Ministry of Education, Culture, Sports, Science and Technology, Japan. We thank two anonymous reviewers for their constructive comments on this manuscript.

Appendix A. Supplementary data

Supplementary data to this article can be found online at https://doi.org/10.1016/j.chemgeo.2020.120031.

References

Abelson, P.H., Hoering, T.C., 1961. Carbon isotope fractionation in formation of amino acids by photosynthetic organisms. Proc. Natl. Acad. Sci. 47, 623–632.
Andersen, N., Paul, H.A., Bernasconi, S.M., McKenzie, J.A., Behrens, A., Schaeffer, P., Albrecht, P., 2001. Large and rapid climate variability during the Messinian salinity crisis: evidence from deuterium concentrations of individual biomarkers. Geology 29, 799–802.
Armellin, S., Brenna, E., Frigoli, S., Fronza, G., Fuganti, C., Mussida, D., 2006. Determination of the synthetic origin of methamphetamine samples by ^{2}H NMR spectroscopy. Anal. Chem. 78, 3113–3117.
Atlas, R.M., 1995. Bioremediation of petroleum pollutants. Int. Biodeterior. Biodegrad. 35, 317–327.
Barna, D., Nagy, B., Csontos, J., Csaszar, A.G., Tasi, G., 2012. Benchmarking experimental and computational thermochemical data: a case study of the butane conformers. J. Chem. Theory Comput. 8, 479–486.
Bayle, K., Gilbert, A., Julien, M., Yamada, K., Silvestre, V., Robins, R.J., Akoka, S., Yoshida, N., Remaud, G.S., 2014. Conditions to obtain precise and true measurements of the intramolecular ^{13}C distribution in organic molecules by isotopic ^{13}C nuclear magnetic resonance spectrometry. Anal. Chim. Acta 846, 1–7.
Becke, A.D., 1993. Density-functional thermochemistry. 3. The role of exact exchange. J. Chem. Phys. 98, 5648–5652.
Bernath, P.F., Bittner, D.M., Sibert, E.L., 2019. Isobutane infrared Bands: Partial Rotational Assignments, ab Initio Calculations, and Local Mode Analysis. J. Phys. Chem. A 123, 6185–6193.
Bigeleisen, J., Mayer, M.G., 1947. Calculation of equilibrium constants for isotopic exchange reactions. J. Chem. Phys. 15, 261–267.
Brenna, E., Fronza, G., Fuganti, C., 2007. Traceability of synthetic drugs by position-specific deuterium isotope ratio analysis - the case of Prozac and the fluoxetine generics. Anal. Chim. Acta 601, 234–239.
Bron, J., Chang, C.F., Wolfsberg, M., 1973. Isotopic partition function ratios involving H_2, H_2O, H_2S, H_2Se, and NH_3. Z. Naturforsch 28a, 129–136.
Byrd, E.F.C., Sherrill, C.D., Head-Gordon, M., 2001. The theoretical prediction of molecular radical species: a systematic study of equilibrium geometries and harmonic vibrational frequencies. J. Phys. Chem. A 105, 9736–9747.
CFOUR, a quantum chemical program package written by J.F. Stanton, J. Gauss, L. Cheng, M.E. Harding, D.A. Matthews, P.G. Szalay with contributions from A.A. Auer, R.J. Bartlett, U. Benedikt, C. Berger, D.E. Bernholdt, Y.J. Bomble, O. Christiansen, F.

Engel, R. Faber, M. Heckert, O. Heun, C. Huber, T. C. Jagau, D. Jonsson, J. Jusélius, K. Klein, W.J. Lauderdale, F. Lipparini, T. Metzroth, L.A. Mück, D.P. O'Neill, D.R. Price, E. Prochnow, C. Puzzarini, K. Ruud, F. Schiffmann, W. Schwalbach, C. Simmons, S. Stopkowicz, A. Tajti, J. Vázquez, F. Wang, J.D. Watts and the integral packages MOLECULE (J. Almlöf and P.R. Taylor), PROPS (P.R. Taylor), ABACUS (T. Helgaker, H.J. Aa. Jensen, P. Jørgensen, and J. Olsen), and ECP routines by A. V. Mitin and C. van Wüllen. For the current version, see http://www.cfour.de., 2000.

Claypool, G.E., Kvenvolden, K.A., 1983. Methane and other Hydrocarbon gases in Marine Sediment. Annu. Rev. Earth Planet. Sci. 11, 299–327.

Cormanich, R.A., Freitas, M.P., 2009. A theoretical view on the conformer stabilization of butane. J. Organomet. Chem. 74, 8384–8387.

Corso, T.N., Brenna, J.T., 1997. High-precision position-specific isotope analysis. Proc. Natl. Acad. Sci. 94, 1049–1053.

Curtis, D.B., Glandorf, D.L., Toon, O.B., Tolbert, M.A., McKay, C.P., Khare, B.N., 2005. Laboratory studies of butane nucleation on organic haze particles: Application to Titan's clouds. J. Phys. Chem. A 109, 1382–1390.

Dobrijevic, M., Loison, J.C., Hickson, K.M., Gronoff, G., 2016. 1D-coupled photochemical model of neutrals, cations and anions in the atmosphere of Titan. Icarus 268, 313–339.

Eiler, J.M., 2013. The Isotopic Anatomies of Molecules and Minerals. Ann. Rev. Earth Planet. Sci. 41, 411–441.

Frisch, M.J., Pople, J.A., Binkley, J.S., 1984. Self-consistent molecular orbital methods. 25. Supplementary functions for Gaussian basis sets. J. Chem. Phys. 80, 3265–3269.

Frisch, M.J., Trucks, G.W., Schlegel, H.B., Scuseria, G.E., Robb, M.A., Cheeseman, J.R., Montgomery Jr., J.A., Vreven, T., Kudin, K.N., Burant, J.C., Millam, J.M., Iyengar, S. S., Tomasi, J., Barone, V., Mennucci, B., Cossi, M., Scalmani, G., Rega, N., Petersson, G.A., Nakatsuji, H., Hada, M., Ehara, M., Toyota, K., Fukuda, R., Hasegawa, J., Ishida, M., Nakajima, T., Honda, Y., Kitao, O., Nakai, H., Klene, M., Li, X., Knox, J.E., Hratchian, H.P., Cross, J.B., Adamo, C., Jaramillo, J., Gomperts, R., Stratmann, R.E., Yazyev, O., Austin, A.J., Cammi, R., Pomelli, C., Ochterski, J.W., Ayala, P.Y., Morokuma, K., Voth, G.A., Salvador, P., Dannenberg, J.J., Zakrzewski, V.G., Dapprich, S., Daniels, A.D., Strain, M.C., Farkas, O., Malick, D.K., Rabuck, A.D., Raghavachari, K., Foresman, J.B., Ortiz, J.V., Cui, Q., Baboul, A.G., Clifford, S., Cioslowski, J., Stefanov, B.B., Liu, G., Liashenko, A., Piskorz, P., Komaromi, I., Martin, R.L., Fox, D.J., Keith, T., Al-Laham, M.A., Peng, C.Y., Nanayakkara, A., Challacombe, M., Gill, P.M.W., Johnson, B., Chen, W., Wong, M. W., Gonzalez, C., Pople, J.A., 2013. Gaussian 09, (Revision D.01). Gaussian, Inc., Wallingford CT.

Galimov, E.M., 1985. The Biological Fractionation of Isotopes. Academic Press, London.

Galimov, E.M., 2006. Isotope organic geochemistry. Org. Geochem. 37, 1200–1262.

Galimov, E.M., Ivlev, A.A., 1973. Thermodynamic isotope effects in organic compounds. I. Carbon isotope effects in straight-chain alkanes. Russ. J. Phys. Chem. 47, 2787–2791 (In Russian).

Gao, L., He, P., Jin, Y., Zhang, Y., Wang, X., Zhang, S., Tang, Y., 2016. Determination of position-specific carbon isotope ratios in propane from hydrocarbon gas mixtures. Chem. Geol. 435, 1–9.

Gilbert, A., Yamada, K., Yoshida, N., 2013a. Accurate Method for the Determination of Intramolecular ^{13}C Isotope Composition of Ethanol from Aqueous Solutions. Anal. Chem. 85, 6566–6570.

Gilbert, A., Yamada, K., Yoshida, N., 2013b. Exploration of intramolecular ^{13}C isotope distribution in long chain n-alkanes (C_{11}-C_{31}) using isotopic ^{13}C NMR. Org. Geochem. 62, 56–61.

Gilbert, A., Yamada, K., Suda, K., Ueno, Y., Yoshida, N., 2016a. Measurement of position-specific ^{13}C isotopic composition of propane at the nanomole level. Geochim. Cosmochim. Acta 177, 205–216.

Gilbert, A., Yamada, K., Yoshida, N., 2016b. Evaluation of on-line pyrolysis coupled to isotope ratio mass spectrometry for the determination of position-specific ^{13}C isotope composition of short chain n-alkanes (C_6-C_{12}). Talanta 153, 158–162.

Gilbert, A., Lollar, B.S., Musat, F., Giunta, T., Chen, S., Kajimoto, Y., Yamada, K., Boreham, C.J., Yoshida, N., Ueno, Y., 2019. Intramolecular isotopic evidence for bacterial oxidation of propane in subsurface natural gas reservoirs. Proc. Natl. Acad. Sci. 116, 6653–6658.

Handy, N.C., Yamaguchi, Y., Schaefer, H.F., 1986. The diagonal correction to the Born-Oppenheimer approximation: its effect on the singlet-triplet splitting of CH_2 and other molecular effects. J. Chem. Phys. 84, 4481–4484.

Harding, M.E., Metzroth, T., Gauss, J., 2008a. Parallel calculation of CCSD and CCSD(T) analytic first and second derivatives. J. Chem. Theory Comput. 4, 64–74.

Harding, M.E., Vázquez, J., Ruscic, B., Wilson, A.K., Gauss, J., Stanton, J.F., 2008b. High-accuracy extrapolated ab initio thermochemistry. III. Additional improvements and overview. J. Chem. Phys. 128, 114111.

Hattori, R., Yamada, K., Kikuchi, M., Hirano, S., Yoshida, N., 2011. Intramolecular carbon isotope distribution of acetic acid in vinegar. J. Agric. Food Chem. 59, 9049–9053.

He, Y., Bao, H., Liu, Y., 2020. Predicting equilibrium intramolecular isotope distribution within a large organic molecule by the cutoff calculation. Geochim. Cosmochim. Acta 269, 292–302.

Huang, F., Daniel, I., Cardon, H., Montagnac, G., Sverjensky, D.A., 2017. Immiscible hydrocarbon fluids in the deep carbon cycle. Nat. Commun. 8, 15798.

Imafuku, Y., Abe, M., Schmidt, M.W., Hada, M., 2016. Heavy element effects in the diagonal Born-Oppenheimer correction within a relativistic spin-free hamiltonian. J. Phys. Chem. A 120, 2150–2159.

Julien, M., Goldman, M.J., Liu, C., Horita, J., Boreham, C.J., Yamada, K., Green, W.H., Yoshida, N., Gilbert, A., 2020. Intramolecular ^{13}C isotope distributions of butane from natural gases. Chem. Geol. 541.

Karton, A., Gruzman, D., Martin, J.M.L., 2009. Benchmark thermochemistry of the C_nH_{2n+2} alkane isomers (n=2-8) and performance of DFT and composite ab initio methods for dispersion-driven isomeric equilibria. J. Phys. Chem. A 113, 8434–8447.

Kinnaman, F.S., Valentine, D.L., Tyler, S.C., 2007. Carbon and hydrogen isotope fractionation associated with the aerobic microbial oxidation of methane, ethane, propane and butane. Geochim. Cosmochim. Acta 71, 271–283.

Kniemeyer, O., Musat, F., Sievert, S.M., Knittel, K., Wilkes, H., Blumenberg, M., Michaelis, W., Classen, A., Bolm, C., Joye, S.B., Widdel, F., 2007. Anaerobic oxidation of short-chain hydrocarbons by marine sulphate-reducing bacteria. Nature 449, 898–U10.

Kolesnikov, A., Kutcherov, V.G., Goncharov, A.F., 2009. Methane-derived hydrocarbons produced under upper-mantle conditions. Nat. Geosci. 2, 566–570.

Kolesnikov, A.Y., Saul, J.M., Kutcherov, V.G., 2017. Chemistry of hydrocarbons under extreme thermobaric conditions. ChemistrySelect 2, 1336–1352.

Krishnan, R., Binkley, J.S., Seeger, R., Pople, J.A., 1980. Self-consistent molecular orbital methods. XX. Basis set for correlated wave-functions. J. Chem. Phys. 72, 650–654.

Lee, C.T., Yang, W.T., Parr, R.G., 1988. Development of the Colle-Salvetti correlation-energy formula into a functional of the electron-density. Phys. Rev. B 37, 785–789.

Li, Y., Zhang, L., Xiong, Y., Gao, S., Yu, Z., Peng, P.A., 2018. Determination of position-specific carbon isotope ratios of propane from natural gas. Org. Geochem. 119, 11–21.

Liu, C., McGovern, G.P., Liu, P., Zhao, H., Horita, J., 2018. Position-specific carbon and hydrogen isotopic compositions of propane from natural gases with quantitative NMR. Chem. Geol. 491, 14–26.

Liu, C., Liu, P., McGovern, G.P., Horita, J., 2019. Molecular and intramolecular isotope geochemistry of natural gases from the Woodford Shale, Arkoma Basin. Oklahoma. Geochim. Cosmochim. Acta 255, 188–204.

Liu, Q., Liu, Y., 2016. Clumped-isotope signatures at equilibrium of CH_4, NH_3, H_2O, H_2S and SO_2. Geochim. Cosmochim. Acta 175, 252–270.

Liu, Q., Tossell, J.A., Liu, Y., 2010. On the proper use of the Bigeleisen-Mayer equation and corrections to it in the calculation of isotopic fractionation equilibrium constants. Geochim. Cosmochim. Acta 74, 6965–6983.

McClurg, R.B., 1999. Comment on "the hindered rotor density-of-states interpolation function" J. Chem. Phys. 106, 6675 (1997) and "the hindered rotor density-of-states" J. Chem. Phys. 108, 2314 (1998). J. Chem. Phys. 111, 7163–7164.

McClurg, R.B., Flagan, R.C., Goddard, W.A., 1997. The hindered rotor density-of-states interpolation function. J. Chem. Phys. 106, 6675–6680.

McLean, A.D., Chandler, G.S., 1980. Contracted Gaussian-basis sets for molecular calculations. 1. 2nd row atoms, Z=11-18. J. Chem. Phys. 72, 5639–5648.

Melzer, E., Schmidt, H.L., 1987. Carbon isotope effects on the pyruvate-dehydrogenase reaction and their importance for relative ^{13}C depletion in lipids. J. Biol. Chem. 262, 8159–8164.

Merrick, J.P., Moran, D., Radom, L., 2007. An evaluation of harmonic vibrational frequency scale factors. J. Phys. Chem. A 111, 11683–11700.

Møller, C., Plesset, M.S., 1934. Note on an approximation treatment for many-electron systems. Phys. Rev. 46, 0618–0622.

Monson, K.D., Hayes, J.M., 1980. Biosynthetic control of the natural abundance of carbon 13 at specific positions within fatty acids in Escherichia coli - evidence regarding the coupling of fatty acid and phospholipid synthesis. J. Biol. Chem. 255, 1435–1441.

Monson, K.D., Hayes, J.M., 1982a. Biosynthetic control of the natural abundance of carbon 13 at specific positions within fatty acids in Saccharomyces cerevisiae - Isotopic fractionations in lipid synthesis as evidence for peroxisomal regulation. J. Biol. Chem. 257, 5568–5575.

Monson, K.D., Hayes, J.M., 1982b. Carbon isotopic fractionation in the biosynthesis of bacterial fatty acids - Ozonolysis of unsaturated fatty acids as a means of determining the intramolecular distribution of carbon isotopes. Geochim. Cosmochim. Acta 46, 139–149.

Murphy, J.E., Vakhtin, A.B., Leone, S.R., 2003. Laboratory kinetics of C_2H radical reactions with ethane, propane, and n-butane at T=96-296 K: implications for Titan. Icarus 163, 175–181.

Piasecki, A., Sessions, A., Lawson, M., Ferreira, A.A., Santos Neto, E.V., Eiler, J.M., 2016a. Analysis of the site-specific carbon isotope composition of propane by gas source isotope ratio mass spectrometer. Geochim. Cosmochim. Acta 188, 58–72.

Piasecki, A., Sessions, A., Peterson, B., Eiler, J., 2016b. Prediction of equilibrium distributions of isotopologues for methane, ethane and propane using density functional theory. Geochim. Cosmochim. Acta 190, 1–12.

Piasecki, A., Sessions, A., Lawson, M., Ferreira, A.A., Neto, E.V.S., Ellis, G.S., Lewan, M. D., Eiler, J.M., 2018. Position-specific ^{13}C distributions within propane from experiments and natural gas samples. Geochim. Cosmochim. Acta 220, 110–124.

Polyakov, V.B., Horita, J., 2021. Equilibrium carbon isotope fractionation factors of hydrocarbons: Semi-empirical force-field method. Chem. Geol. 559, 119948.

Pople, J.A., Headgordon, M., Raghavachari, K., 1987. Quadratic configuration interaction - a general technique for determining electron correlation energies. J. Chem. Phys. 87, 5968–5975.

Purvis, G.D., Bartlett, R.J., 1982. A full coupled-cluster singles and doubles model - the inclusion of disconnected triples. J. Chem. Phys. 76, 1910–1918.

Reeves, E.P., Seewald, J.S., Sylva, S.P., 2012. Hydrogen isotope exchange between n-alkanes and water under hydrothermal conditions. Geochim. Cosmochim. Acta 77, 582–599.

Richet, P., Bottinga, Y., Javoy, M., 1977. A review of hydrogen, carbon, nitrogen, oxygen, Sulphur, and chlorine stable isotope fractionation among gaseous molecules. Annu. Rev. Earth Planet. Sci. 5, 65–110.

Riley, K.E., Pitonak, M., Jurecka, P., Hobza, P., 2010. Stabilization and Structure Calculations for Noncovalent Interactions in Extended Molecular Systems based on Wave Function and Density Functional Theories. Chem. Rev. 110, 5023–5063.

Rustad, J.R., 2009. Ab initio calculation of the carbon isotope signatures of amino acids. Org. Geochem. 40, 720–723.
Schauble, E.A., 2004. Applying stable isotope fractionation theory to new systems. Rev. Mineral. Geochem. 55, 65–111.
Schauer, J.J., Kleeman, M.J., Cass, G.R., Simoneit, B.R.T., 1999. Measurement of emissions from air pollution sources. 2. C_1 through C_{30} organic compounds from medium duty diesel trucks. Environ. Sci. Technol. 33, 1578–1587.
Seewald, J.S., 1994. Evidence for metastable equilibrium between hydrocarbons under hydrothermal conditions. Nature 370, 285–287.
Seewald, J.S., 2001. Aqueous geochemistry of low molecular weight hydrocarbons at elevated temperatures and pressures: Constraints from mineral buffered laboratory experiments. Geochim. Cosmochim. Acta 65, 1641–1664.
Seewald, J.S., 2003. Organic-inorganic interactions in petroleum-producing sedimentary basins. Nature 426, 327–333.
Sessions, A.L., Sylva, S.P., Summons, R.E., Hayes, J.M., 2004. Isotopic exchange of carbon-bound hydrogen over geologic timescales. Geochim. Cosmochim. Acta 68, 1545–1559.
Shimanouchi, T., 1977. Tables of molecular vibrational frequencies, Consolidated volume II. J. Phys. Chem. Ref. Data 6, 993–1102.
Singh, R., Guzman, M.S., Bose, A., 2017. Anaerobic Oxidation of Ethane, Propane, and butane by Marine Microbes: a Mini Review. Front. Microbiol. 8, 2056.
Suda, K., Gilbert, A., Yamada, K., Yoshida, N., Ueno, Y., 2017. Compound- and position-specific carbon isotopic signatures of abiogenic hydrocarbons from on-land serpentinite-hosted Hakuba Happo hot spring in Japan. Geochim. Cosmochim. Acta 206, 201–215.
Thiagarajan, N., Xie, H., Ponton, C., Kitchen, N., Peterson, B., Lawson, M., Formolo, M., Xiao, Y., Eiler, J., 2020. Isotopic evidence for quasi-equilibrium chemistry in thermally mature natural gases. Proc. Natl. Acad. Sci. 117, 3989–3995.
Urey, H.C., 1947. The thermodynamic properties of isotopic substances. J. Chem. Soc. (Lond.) 562–581.
Vogler, E.A., Hayes, J.M., 1980. Carbon isotopic compositions of carboxyl groups of biosynthesized fatty acids. Phys. Chem. Earth 12, 697–704.
Wang, Y., Sessions, A.L., Nielsen, R.J., Goddard III, W.A., 2009a. Equilibrium $^2H/^1H$ fractionations in organic molecules. II: Linear alkanes, alkenes, ketones, carboxylic acids, esters, alcohols and ethers. Geochim. Cosmochim. Acta 73, 7076–7086.
Wang, Y., Sessions, A.L., Nielsen, R.J., Goddard III, W.A., 2009b. Equilibrium $^2H/^1H$ fractionations in organic molecules: I. Experimental calibration of ab initio calculations. Geochim. Cosmochim. Acta 73, 7060–7075.
Wang, Y., Sessions, A.L., Nielsen, R.J., Goddard III, W.A., 2013. Equilibrium $^2H/^1H$ fractionation in organic molecules: III. Cyclic ketones and hydrocarbons. Geochim. Cosmochim. Acta 107, 82–95.
Webb, M.A., Miller III, T.F., 2014. Position-specific and clumped stable isotope studies: comparison of the Urey and path-integral approaches for carbon dioxide, nitrous oxide, methane, and propane. J. Phys. Chem. A 118, 467–474.
Xie, H., Ponton, C., Formolo, M.J., Lawson, M., Peterson, B.K., Lloyd, M.K., Sessions, A. L., Eiler, J.M., 2018. Position-specific hydrogen isotope equilibrium in propane. Geochim. Cosmochim. Acta 238, 193–207.
Yamada, K., Kikuchi, M., Gilbert, A., Yoshida, N., Wasano, N., Hattori, R., Hirano, S., 2014. Evaluation of commercially available reagents as a reference material for intramolecular carbon isotopic measurements of acetic acid. Rapid Commun. Mass Spectrom. 28, 1821–1828.
Yang, H., Huang, Y.S., 2003. Preservation of lipid hydrogen isotope ratios in Miocene lacustrine sediments and plant fossils at Clarkia, northern Idaho. USA. Org. Geochem. 34, 413–423.
Yoshida, N., Toyoda, S., 2000. Constraining the atmospheric N_2O budget from intramolecular site preference in N_2O isotopomers. Nature 405, 330–334.
Zhang, J., Liu, X., Blume, R., Zhang, A.H., Schlogl, R., Su, D.S., 2008. Surface-modified carbon nanotubes catalyze oxidative dehydrogenation of n-butane. Science 322, 73–77.
Zhang, Y., Liu, Y., 2018. The theory of equilibrium isotope fractionations for gaseous molecules under super-cold conditions. Geochim. Cosmochim. Acta 238, 123–149.
Zhao, Y., Truhlar, D.G., 2008. The M06 suite of density functionals for main group thermochemistry, thermochemical kinetics, noncovalent interactions, excited states, and transition elements: two new functionals and systematic testing of four M06-class functionals and 12 other functionals. Theor. Chem. Accounts 120, 215–241.